

Semiparametric Inference of Effective Reproduction Number Dynamics from Wastewater Pathogen Surveillance Data

Isaac H. Goldstein¹, Daniel M. Parker², Sunny Jiang³, Volodymyr M. Minin¹

¹Department of Statistics, University of California, Irvine

²Department of Population Health and Disease Prevention; Department of Epidemiology and Biostatistics, University of California, Irvine

³Department of Civil and Environmental Engineering; Department of Ecology and Evolutionary Biology, University of California, Irvine

Abstract

Concentrations of pathogen genomes measured in wastewater have recently become available as a new data source to use when modeling the spread of infectious diseases. One promising use for this data source is inference of the effective reproduction number, the average number of individuals a newly infected person will infect. We propose a model where new infections arrive according to a time-varying immigration rate which can be interpreted as a compound parameter equal to the product of the proportion of susceptibles in the population and the transmission rate. This model allows us to estimate the effective reproduction number from concentrations of pathogen genomes while avoiding difficult to verify assumptions about the dynamics of the susceptible population. As a byproduct of our primary goal, we also produce a new model for estimating the effective reproduction number from case data using the same framework. We test this modeling framework in an agent-based simulation study with a realistic data generating mechanism which accounts for the time-varying dynamics of pathogen shedding. Finally, we apply our new model to estimating the effective reproduction number of SARS-CoV-2 in Los Angeles, California, using pathogen RNA concentrations collected from a large wastewater treatment facility.

1 Introduction

For many pathogens, infected individuals will shed copies of the pathogen through fecal matter over the course of their infection. Viral gene concentrations measured in wastewater samples are a noisy aggregate of the concentrations of genomes generated by infected individuals connected to the wastewater system, and thus provide insight into the dynamics of the spread of an infectious disease. While viral gene concentrations collected in wastewater samples have recently become widely available, statistical methods for utilizing such data are in their infancy. One promising use for pathogen genome concentrations as data is estimation of the effective reproduction number. The effective reproduction number (R_t), the average number of individuals an infectious person at time t would subsequently infect, is a useful way of describing the state of an infectious disease epidemic. When R_t is below 1, we expect the number of new infections to decrease; the reverse is true when R_t is above 1. Statistical models that use observed data to produce timely and accurate estimates of the effective reproduction number from surveillance data (data collected through passive public health surveillance) have an important role to play in an effective public health response to an epidemic. In this paper, we develop a new method for estimating the effective reproduction number from pathogen genome concentrations collected from wastewater, and as a bi-product, show how this method can be used to estimate the effective reproduction number from case data as well.

Recently, a number of studies have shown SARS-CoV-2 (the causative agent of COVID-19) RNA concentrations measured in wastewater provide meaningful information about the spread of SARS-CoV-2. For instance, Morvan et al. [24] show that estimates of prevalence based on wastewater RNA closely match estimates based on household prevalence surveys. At a much smaller scale, Acer et al. [1] show that SARS-CoV-2 concentrations passively collected outside of a university isolation hall correspond with the number of infected individuals inside the building. Many other studies show SARS-CoV-2 RNA concentrations can correlate with reported cases of COVID-19 [31, 42]. Zulli et al. [44] show that SARS-CoV-2 RNA also correlates well with case rates. Wade et al. [36] provide a useful introduction to the many sources of uncertainty in the pathogen genome concentration data generation process.

From the perspective of inferential methods, pathogen genome concentrations are a potentially less biased data source than other data sources such as counts of new cases, which can be biased by policies regarding testing availability and the willingness of the population to test [20]. To our knowledge, there have been relatively few attempts to use pathogen genome concentrations collected from wastewater (henceforth referred to as wastewater data) to estimate the effective reproduction number. Huisman et al. [18] adapted their case based method [17] and used SARS-CoV-2 wastewater data to create a synthetic time series of hypothetical case data, which is then analyzed with the widely used case-based method `EpiEstim` [7]. Because the model uses a branching process inspired method, it has relatively few parameters which must be specified by the user. One disadvantage of this approach is that the synthetic incidence is truncated in order to avoid issues of right-censoring, making it impossible to provide real time inference. Nourbakhsh et al. [25] used a classic compartmental model where RNA concentrations were modeled as noisy realization of the number of currently infectious and recently recovered individuals. Unlike the Huisman et al. [18] method, the Nourbakhsh et al. [25] models multiple stages of infection and recovery, as well as the effects of the sewer system on the observed data. In part due to this complexity, it requires a number of parameters to be specified by users in order to produce inference, many of which are difficult to verify in practice. One advantage of this approach is that it produces inference on many more quantities than just the effective reproduction number.

Taking inspiration from previous work on non-parametric modeling of the transmission rate in compartmental models [41] and birth-death modeling in infectious disease phylodynamics [32], we introduce a simpler compartmental model with only compartments needed to estimate the effective reproduction number and equip it with a Bayesian nonparametric inference framework. This simpler model combined with our Bayesian nonparametric framework lets us avoid some difficult-to-verify assumptions, while still estimating the effective reproduction number from wastewater data.

In this paper, we first introduce the classic compartmental modeling framework, then our new wastewater-based method for estimating the effective reproduction number. We test our new model against compartmental models fit to case and wastewater data as well as a state-of-the-art wastewater-based method on simulated data. Finally, we apply our new method to estimate the effective reproduction number of SARS-CoV-2 in Los Angeles, California using SARS-CoV-2 RNA concentrations collected from a large wastewater treatment plant.

Table 1: Parameters of the SEIR model.

Parameter	Interpretation
β_t	time-varying transmission rate
$1/\gamma$	average time infected but not infectious (average length of the latent period)
$1/\nu$	average length of the infectious period

2 Methods

2.1 Available data

We will consider two types of surveillance data; concentrations of pathogen genomes measured in wastewater, and reported new cases, observed at times t_1, \dots, t_T .

It is common practice to measure the concentration from the same sample of wastewater multiple times, producing multiple measurements called replicates. In real world data sets, an average of replicates is often reported. We will consider both raw concentrations and averages in this study.

We define $\mathbf{X} = (X_{t_1,1}, \dots, X_{t_1,j}, \dots, X_{t_T,j})$, where $X_{t_i,j}$ is the j th replicate of pathogen genomes collected from wastewater at time t_i , with units of copies per milliliter. We will model $X_{t_i,j}$ as a noisy representation of the unobserved number of currently infectious and recently recovered individuals.

Let $\mathbf{O} = (O_{t_1}, O_{t_2}, O_{t_3}, \dots, O_{t_T})$, where O_{t_u} is the number of newly observed cases of an infectious disease during time interval $(t_{u-1}, t_u]$. We will model O_{t_u} as a noisy realization of the number of individuals transitioning from the latent stage of infection to the infectious stage.

2.2 Standard compartmental models

An SEIR compartmental model describes a homogeneously mixing population moving through stages of infectious disease, referred to as compartments. The compartments are S , susceptible individuals; E , infected but not yet infectious individuals; I , currently infectious individuals; and R , no longer infectious either due to recovery or death. In its deterministic form, the changes in the number of individuals in these compartments are described using a system of ordinary differential equations (ODEs). The behavior of the ODEs is described by a set of key parameters defined in Table 1. The SEIR system of ODEs is:

$$\begin{aligned} \frac{dS}{dt} &= -\beta_t \times I \times S/N, & \frac{dI}{dt} &= \gamma \times E - \nu \times I, \\ \frac{dE}{dt} &= \beta_t \times I \times S/N - \gamma \times E, & \frac{dR}{dt} &= \nu \times I. \end{aligned}$$

We model β_t as time-varying to account for changes in transmission due to, for example, implementation of public health policies, changes in behavior, or the emergence of new pathogen variants.

For the SEIR model, the time-varying basic reproduction number, $R_{0,t}$, the average number of individuals a person infected at time t would infect in a completely susceptible population, and effective reproduction number, R_t , are defined as:

$$R_{0,t} = \frac{\beta_t}{\nu}, \quad R_t = R_{0,t} \times \frac{S(t)}{N}.$$

We will adapt this classic model for our purpose of estimating the effective reproduction number from wastewater data.

2.3 The EIRR model

To use an SEIR model for inference, we must specify the initial number of susceptibles at the start of the observation period. Doing so requires accurate estimates of the cumulative number of infections, and, for diseases where individuals can be re-infected, accurate estimates of the number of individuals who have recovered and become susceptible again. Estimating those quantities from observed data is itself a non-trivial task. In addition, modeling waning immunity (i.e. allowing for transitions from the R to the S compartment) becomes especially problematic when accounting for new pathogen variants, which can cause the rates of waning immunity to change.

Taking inspiration from birth-death modeling in infectious disease phylodynamics [32], we define $\alpha_t = \beta_t \times S/N$ and rewrite the equation for $\frac{dE}{dt}$ so that:

$$\frac{dE}{dt} = \alpha_t \times I - \gamma \times E.$$

The rate of new latent infections no longer depends on the S compartment. Note, the effective reproduction number is still recoverable, as $R_t = \frac{\beta_t S(t)}{\nu N} = \frac{\alpha_t}{\nu}$.

In addition, we split the R compartment in two. In the first compartment individuals are recovered but still shedding pathogen genomes, in the second they are recovered and no longer shedding genomes. This choice is motivated by the characteristics of SARS-CoV-2, for which it has been shown individuals shed detectable amounts of RNA in fecal matter well after the likely end of their infectious period (see Web Section A.2.3) [26, 43]. The final model, which we call the EIRR model, is described by the following equations:

$$\begin{aligned} \frac{dE}{dt} &= \alpha_t \times I - \gamma \times E, & \frac{dR1}{dt} &= \nu \times I - \eta \times R1, \\ \frac{dI}{dt} &= \gamma \times E - \nu \times I, & \frac{dR2}{dt} &= \eta \times R1. \end{aligned}$$

For the sake of comparison, we will also implement the SEIRR model, which is the SEIR model with two R compartments.

2.4 Wastewater observation model

We model the log of observed pathogen genome concentrations as realizations of the following generalized t-distribution:

$$\log X_{t_i,j} \sim \text{Generalized t}(\log(\lambda \times I(t_i) + (1 - \lambda) \times R1(t_i)) + \log(\rho), \tau^2, df).$$

Here $I(t_i)$ is the number of currently infectious individuals at time t_i , $R1(t_i)$ is the number of non-infectious but still shedding individuals at time t_i . The t_i do not have to be regularly spaced; data can be collected at irregular intervals so long as the system of ODEs is solved at a finer resolution than the smallest interval length. The parameter λ is a normalized weight representing how much each individual contributes to the true underlying pathogen genome concentrations while infectious. Parameter ρ allows for flexibility in relating counts of individuals to concentrations. Parameter τ accounts for variation from the mean, and df

is the parameter governing the degrees of freedom of the t-distribution. We chose to use a t-distribution because wastewater data often has many outliers; a t-distribution with thicker tails should better fit the data as opposed to the normal distribution.

2.5 Choosing a λ prior for SARS-CoV-2 using a stochastic SEIRR

We used a simulation study in order to elicit an appropriate prior for λ . We simulated 1000 epidemics from an agent-based stochastic SEIRR model (the stochastic equivalent to an SEIR model with two R compartments, see Web Section A.2.1), where the times of each individual’s transitions between different model states were recorded. For individual i in the I or $R1$ state infected at time t_i , the concentration of pathogen genomes associated with their shedding at time l is modeled as a random variable $Z_i(t_i, l)$, where

$$Z_i(t_i, l) \sim 10^{\text{Normal}(\mu_i(l-t_i), 1.09)}$$

and the value of $\mu_i(l - t_i)$ was calculated using the consensus shedding load profile of SARS-CoV-2 pathogen RNA generated in [25] by synthesizing previous studies [2, 23, 16]. The value 1.09 is the average variation in genome concentrations on the log base 10 scale amongst individuals over the course of an infection. We calculated this global average variation in concentrations by averaging over the empirical standard deviations of SARS-CoV-2 RNA shed by individuals 6 to 22 days after symptom onset, using the data available from [16], which uses data collected by Wölfel et al. [39], Han et al. [14], and Lui et al. [21]. The population level concentration of genomes at time l was the sum of all the individual genome concentrations in the I and $R1$ states at time l divided by the total population size. The total concentration depends on the parameters governing the time individuals spend in the I and $R1$ compartments. To account for a wide range of plausible scenarios, for each simulation, γ , ν and η were chosen from the priors we used when fitting the EIRR model to SARS-CoV-2 data (Table A2). Then, for each simulation, we fit a linear model (constrained to positive coefficients using a method described in [10]):

$$E[\text{Total genome concentration}] = \beta_1 \times \text{Prevalence in } I + \beta_2 \times \text{Prevalence in } R1$$

and calculated $\lambda = \beta_1 / (\beta_1 + \beta_2)$. We then found a logit-normal prior for λ which matches the 95% quantiles of these 1000 λ values by minimizing the squared error of the logit-normal prior quantiles and the 95% quantiles from our 1000 λ values using the Nelder-Mead algorithm implemented in the `optim` function in R [27]. Further details of the simulation protocol are available in Appendix Sections A.2.1 and A.2.3.

2.6 Complete EIRR-ww model structure

We describe the complete wastewater data model, which we call the EIRR-ww model, structure in the following section. We use a random walk prior for the time-varying effective reproduction number:

$$\begin{aligned} R_0 &\sim \text{Log-Normal}(\mu_0, \sigma_0), \\ \sigma &\sim \text{Log-Normal}(\mu_{rw}, \sigma_{rw}), \\ \log(R_{k_i}) | R_{k_{i-1}}, \sigma &\sim \text{Normal}(\log(R_{k_{i-1}}), \sigma). \end{aligned}$$

The times k_i can be chosen flexibly, for this study, we choose them so that R_t changes on a weekly basis. We also choose priors for the initial counts in each compartment, rate parameters, and observation model parameters independently. Let $\bar{\Theta} = (\gamma, \nu, \eta, I(0), E(0), R1(0))$ and $\mathbf{R} = (R_{k_1}, \dots, R_{k_M})$ be the vector of effective reproduction number values. Let

$$M(t, \bar{\Theta}, \mathbf{R}) = (\mathbf{E}(t, \bar{\Theta}, \mathbf{R}), \mathbf{I}(t, \bar{\Theta}, \mathbf{R}), \mathbf{R1}(t, \bar{\Theta}, \mathbf{R}), \mathbf{R2}(t, \bar{\Theta}, \mathbf{R}))$$

be the solution to the EIRR ODE system described in section 2.3. The target posterior distribution is:

$$P(\mathbf{R}, \bar{\Theta}, \rho, \lambda, \tau, df, \sigma \mid \mathbf{X}) \propto \underbrace{P(\mathbf{X} \mid \mathbf{M}(t, \bar{\Theta}, \mathbf{R}), \rho, \lambda, \tau, df)}_{\text{Concentration Model}} \underbrace{P(\mathbf{R} \mid \sigma)}_{\text{RW Prior}} P(\bar{\Theta}, \rho, \lambda, \tau, df, \sigma).$$

We use the No-U-Turn Sampler, implemented in the `Julia` package `turing` to approximate this posterior distribution [15, 11]. We used non-centered re-parameterizations for all model parameters except for df (which had a gamma prior). Markov chain Monte Carlo chains were initialized using the Maximum A Posterior (MAP) estimate of each parameter plus Gaussian noise (except for df which was only initialized at the MAP).

2.7 The EIR model

The EIRR model can be simplified further when fitting to case data by using only a single R compartment (because we don't need to model different stages of recovery), creating the EIR model. The EIR Model is described by the following series of equations:

$$\begin{aligned} \frac{dE}{dt} &= \alpha_t \times I - \gamma \times E, & \frac{dR}{dt} &= \nu \times I, \\ \frac{dI}{dt} &= \gamma \times E - \nu \times I, & \frac{dC}{dt} &= \gamma \times E. \end{aligned}$$

The redundant compartment C counts cumulative transitions from the E to I compartments, in order to connect the EIR model to observed case data.

2.8 Case observation model

We model observed cases as a noisy realization of the number of transitions from the E compartment to the I compartment. For cases observed in the interval $(t_{u-1}, t_u]$:

$$O_u \sim \text{Negative-Binomial}((C(t_u) - C(t_{u-1})) \times \psi, \phi),$$

where $C(t_u) - C(t_{u-1})$ is the number of transitions from the E to the I compartment in time interval $(t_{u-1}, t_u]$, ψ is a detection rate parameter, and ϕ is an over-dispersion parameter. Both ψ and ϕ have their own priors.

The full structure of our case model, the EIR-cases model, is otherwise very similar to the EIRR-ww model. The structures of the corresponding SEIR-cases/SEIRR-ww models are likewise similar, though for SEIR-cases/SEIRR-ww models the basic reproduction number is modeled as random walk, rather than the effective reproduction number. We provide a more detailed description of the SEIRR-ww model priors in Appendix Section A.1.1. All code used to produce this paper is available at https://github.com/igoldsteinh/ww_paper. A `Julia` package implementing the models used in this paper is available at <https://github.com/igoldsteinh/concRt.jl>. An `R` package which provides a wrapper for the `Julia` package is available at <https://github.com/igoldsteinh/concRt>.

2.9 State-of-the-art methods

We compare the EIRR-ww model to the Huisman et al. [18] method. This method is a variation on the well known `EpiEstim` method [7]. First, pathogen genome concentrations are translated into synthetic incidence counts via a convolution equation. Next, these synthetic counts are passed into `EpiEstim`. Users of this method must both specify a shedding load profile to de-convolve concentrations into incidence, as well as a generation time distribution to relate incidence to the effective reproduction number. See Huisman et al. [18] for details. In contrast, the method of Nourbakhsh et al. [25] uses a compartmental model similar to ours, splitting both the I and $R1$ compartments into many smaller compartments in order to better match the shedding dynamics of pathogen genomes in fecal matter. They also directly model the impact of the sewer system itself on the final observed data. We decided not to test the method of Nourbakhsh et al. [25] in this study because the code for the latter method is not readily available, and because the goal of their model was not limited to inference of the effective reproduction number.

3 Results

3.1 Simulation protocol

We simulated a single realization from the agent-based stochastic SEIRR described in section 2.5. The population size was set to 100,000. The mean latent period was 4 days, the mean infectious period was 7 days, and the mean time spent recovered but still shedding pathogen genomes was 18 days. The simulation was started with 200 individuals in each of the E and I compartments, and run for a warm-up period of 77 days before creating data for the model to fit to. This was done so that there would be individuals in all compartments for whom all transition times between compartments would be naturally available. The top left panel of Figure 1 shows the prevalence in each compartment, the time 0 is the day before the first wastewater sample is collected.

The basic reproduction number $R_{0,t}$ was given a fixed trajectory. We calculated the true R_t at each day using the formula in Section 2.2. For the observation period, we chose to start with $R_{0,t}$ set to 0.9 with a rapid increase to 2.5, where it stayed for the duration of the simulation, mimicking a scenario where a new and highly infectious variant is introduced into a population. All priors used in the simulation are listed in Table A2 (for the case models the priors for γ and ν are transformed to be on a weekly scale).

Using this single realization from the stochastic SEIRR model, we simulated 100 data sets of pathogen genome concentrations and 100 data sets of observed case data. We chose to use only one realization so that the trajectory of R_t , which depends on the changes in the susceptible population, would be fixed across all 100 simulations, allowing us to report properly defined frequentist metrics. Different compartment count realizations from the SEIRR model should not result in substantially different simulation results because in our relatively large population size setting stochastic compartmental model trajectories should be close to their asymptotic expectations defined by the corresponding system of ODEs. All parameters were chosen to create data similar to observed data from the SARS-CoV-2 pandemic in Los Angeles, California (see the Appendix for more details). Daily genome concentration data was generated using a generalized t-distribution as in the model described in Section 2.4. However, the mean of the generalized t-distribution was the true total genome concentration shed, generated using the method described in Section 2.5. We simulated ten

replicates per day. Parameter ρ was set to be 0.011, τ was set to be 0.5, and df was set to 2.99. Only data from every other day were used for analysis.

Cases were simulated at a daily time-scale and aggregated to a weekly time-scale. The case detection rate ψ was set to 0.2, while ϕ was set to 57.55. We generated data for a total of 19 weeks. While the case likelihood of our SEIR-cases and EIR-cases models is quite similar to the data generating mechanism of the simulated data, the wastewater likelihood of our SEIRR-ww and EIRR-ww models is a crude approximation of the data generating mechanism of the simulated data. For all subsequent simulation scenarios, we use the same 100 data sets while changing either the type of data used to fit the model, or the model priors.

In the baseline simulation scenario, we fit the SEIR-cases, EIR-cases, SEIRR-ww and EIRR-ww models to the data, using three replicates for the wastewater models and weekly cases for the case models. In subsequent scenarios, we only fit the EIRR-ww model. Using the same priors as in the baseline scenario, we fit the EIRR-ww model using one or ten replicates instead of three replicates (1-rep and 10-rep) and also fit the model using the mean of three replicates or the mean of ten replicates (3-mean and 10-mean respectively). We also conduct sensitivity analyses where the priors for the initial E and I compartments are centered at 75% or 133% of true values (Low Init and High Init respectively). We shift the prior for λ so that it is centered around 0.8 (Low Prop) as opposed to the default 0.99. Finally, we fit the Huisman method using the mean of three replicates as the input data. To choose a shedding load profile, we first re-fit a spline to the points from the Nourbakhsh et al. [25] profile raised to the tenth power, with an additional value of 0 at time 0. We then generated predictions from the spline from 0 to 29 evenly spaced by 0.1, and used these as true values from the shedding load profile. We then used the Nelder-Mead algorithm to search for shape and scale parameters of the gamma distribution which minimized the squared loss of the proposed grid point values versus our generated true values, and used these parameters as the shape and scale of the shedding load profile for the Huisman model. In an SEIR model, the intrinsic generation time distribution is the sum of the latent and infectious periods [33, 5, 6], which is a hypo-exponential distribution. `EpiEstim` is normally used assuming the generation time distribution is a gamma distribution. We used a gamma distribution with mean and standard deviation equal to the true intrinsic generation time distribution. Note that for the Huisman method, because the method relies on generating a synthetic series of cases, the method truncates the inferred R_t values in order to only infer R_t for times for which the method believes there are enough pathogen genome concentrations available to correctly generate synthetic cases. Also, `EpiEstim` does not estimate the effective reproduction number for early points in the time-series. When comparing the Huisman method to the baseline EIRR-ww model, we restrict the comparison to only be on time points for which both models produced inference.

An example realization of the simulation is displayed in Figure 1. All priors used in the baseline simulation are listed in Table A2.

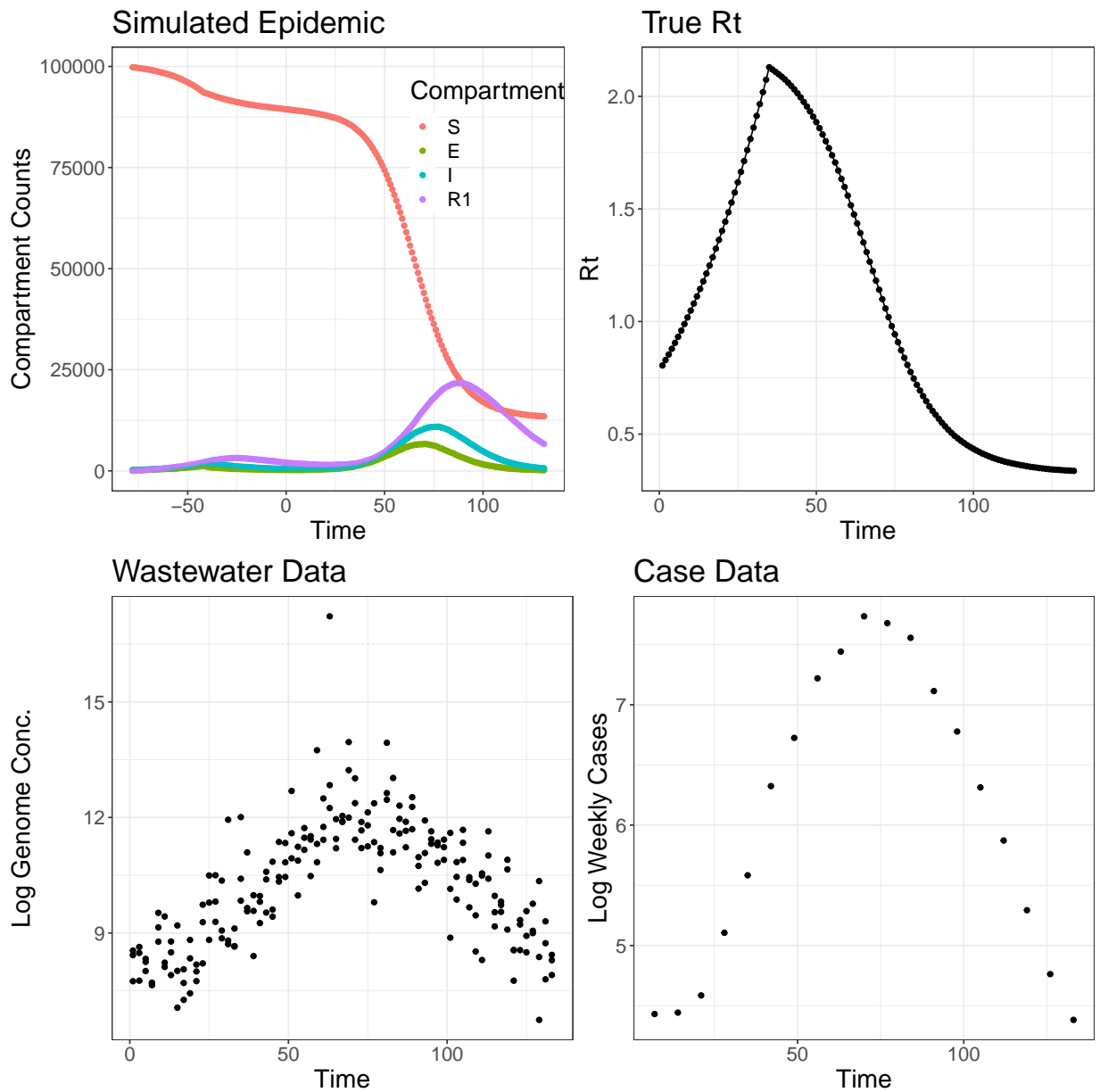


Figure 1: An example of simulated epidemic data generated from a single realization of a stochastic SEIRR model. Top left panel shows the simulated epidemic, time 0 is the day before the first wastewater sample/case is observed. Top right panel shows the true effective reproduction number trajectory. Bottom row shows simulated wastewater and case data on the log scale.

3.2 Simulation results

3.2.1 Baseline simulation

Posterior medians and credible intervals for models fit to the example simulation data are displayed in Figure 2.

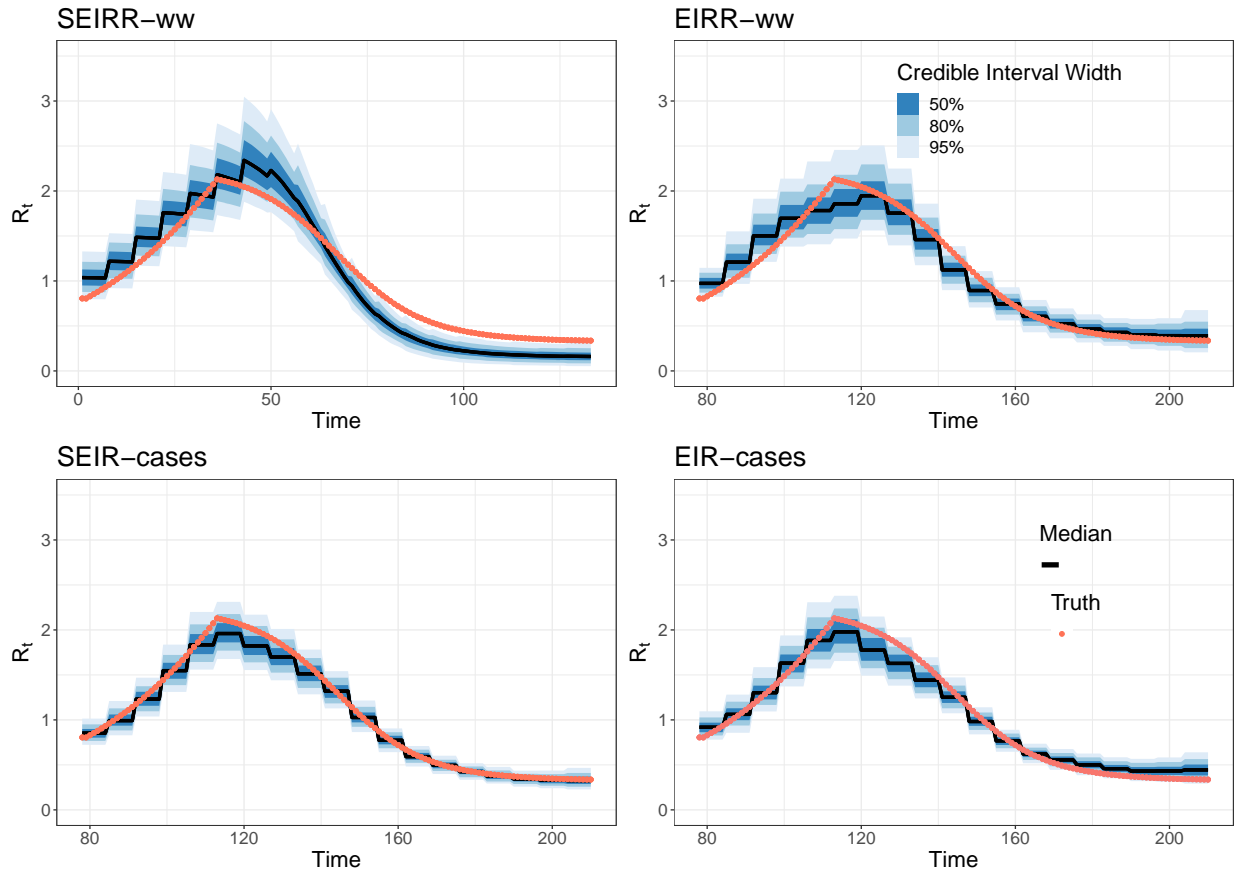


Figure 2: Posterior summaries of R_t using four models fit to either wastewater or case data generated from the same underlying infectious disease dynamics. True R_t trajectories are colored in red, black lines represent posterior medians, blue shaded areas from dark to light are 50, 80 and 95% credible intervals. Models in the top row use genome concentrations, models in the bottom row use case counts. Models in the left column use the S compartment, models in the right column do not.

Posterior trajectories from all models generally mimic the true R_t curve, although the SEIRR-ww model struggles to capture the exact trajectory. Models using genome concentrations have wider credible intervals than models using case counts, reflecting higher variability of wastewater data as compared to case data. Note that the random walk prior forces R_t to change on a weekly scale, while the true values are reported on a daily scale. This results in more pronounced segmentation of posterior summaries. The SEIRR-ww model (top left of Figure 1) estimates sloping spikes because the SEIRR ODEs are solved at a daily time scale, meaning that for a fixed weekly R_0 there are seven estimates of the number of susceptibles and effective reproduction numbers. This behavior is missing from the SEIR-cases model because the SEIR ODEs are solved at a weekly time scale. EIRR-ww posterior estimates of the latent trajectories (including latent incidence) are displayed in Appendix Figure A7. While posterior estimates mimic the shape of the latent trajectories, they fail to capture the magnitude of the trajectories except at the beginning and end of the simulation.

To assess performance across many simulated data sets, we examined frequentist properties of our four models, summarised in Figure 3. Boxplot solid lines represent medians, hinges are upper and lower quartiles and whiskers are at most 1.5 times the inter-quartile range from the median. Envelope is a measure of coverage. For each simulation the envelope

is the proportion of time points for which an 80% credible interval from the posterior distribution captured the true value of interest. Ideally it should be 0.8. We chose to use 80% credible intervals as estimates of the 80% quantiles have less Monte Carlo Error than 95% quantiles, so fewer data sets are needed to estimate them well. We include the corresponding 95% credible interval results in Appendix Figure A10. Mean credible interval width (MCIW) is the mean of 80% credible interval widths across time points within a simulation. Absolute deviation is a measure of bias, and is the mean of the absolute difference between the posterior median and the true value at each time point. Finally, mean absolute sequential variation (MASV) measures how well each method captures the variation in the effective reproduction number across time by computing the mean of the absolute difference between the posterior median at t and the posterior median at $t - 1$. We compare this to the true mean absolute sequential variation in each simulation. The EIRR-ww model outperforms the SEIRR-ww model in terms of bias, precision, and coverage. Both the SEIR-cases model and the EIR-cases model outperform the EIRR-ww model in terms of bias and precision. The EIR-cases model is slightly more biased and less precise than the SEIR-cases model. Although the EIRR-ww model has less precision than case based models, this simulation shows that models using wastewater data can be used to estimate the effective reproduction number reasonably well.

Frequentist Metrics Across Models

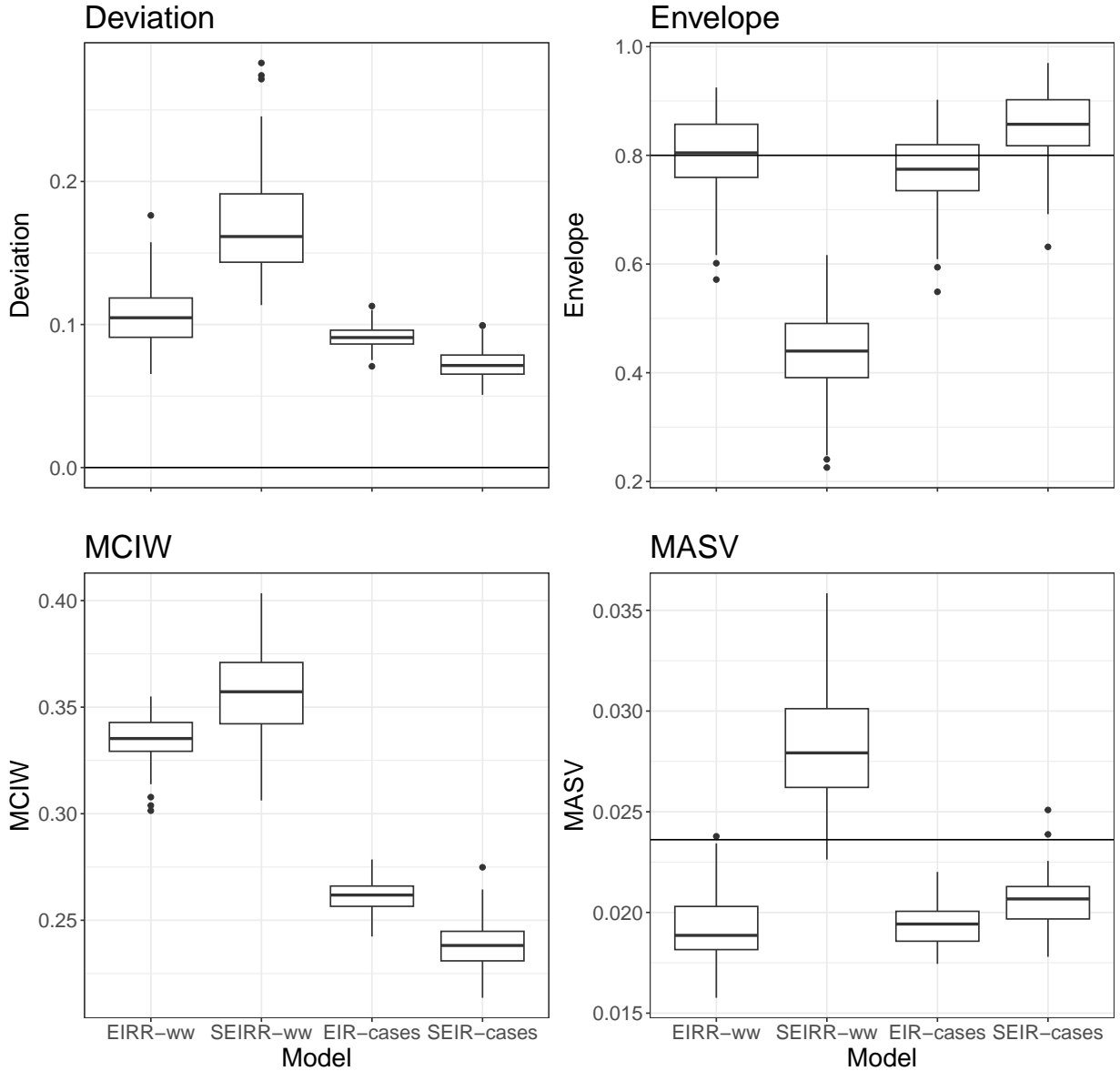


Figure 3: Frequentist metrics for the EIRR-ww, SEIRR-ww, EIR-cases and SEIR-cases models in the baseline scenario. Absolute deviation is the mean of the absolute value of the difference between the median R_t at each time point and the true value. Envelope is a measure of coverage, taking the average coverage of 80% intervals over the time series. MCIW is the average mean credible interval width. Mean absolute standard deviation (MASV) is the difference between the current median point estimate for R_t and the previous point estimate for R_t . The line in the bottom right panel represents the true absolute standard deviation. Solid lines represent medians, hinges are upper and lower quartiles and whiskers are at most 1.5 times the inter-quartile range from the median.

3.2.2 Performance across different kinds of simulated wastewater data

Frequentist metrics comparing the baseline EIRR-ww fit (three replicates) to the EIRR-ww fit to one and ten replicates, and to the EIRR-ww fit to mean of three replicates and mean of

ten replicates, are displayed in Figure 4. The EIRR-ww fit to one or ten replicates performed modestly worse or better respectively than the EIRR-ww fit to three replicates. The EIRR-ww fit to raw replicate concentrations performed slightly better than the EIRR-ww fit to means of replicates.

Frequentist Metrics Across Data Sources

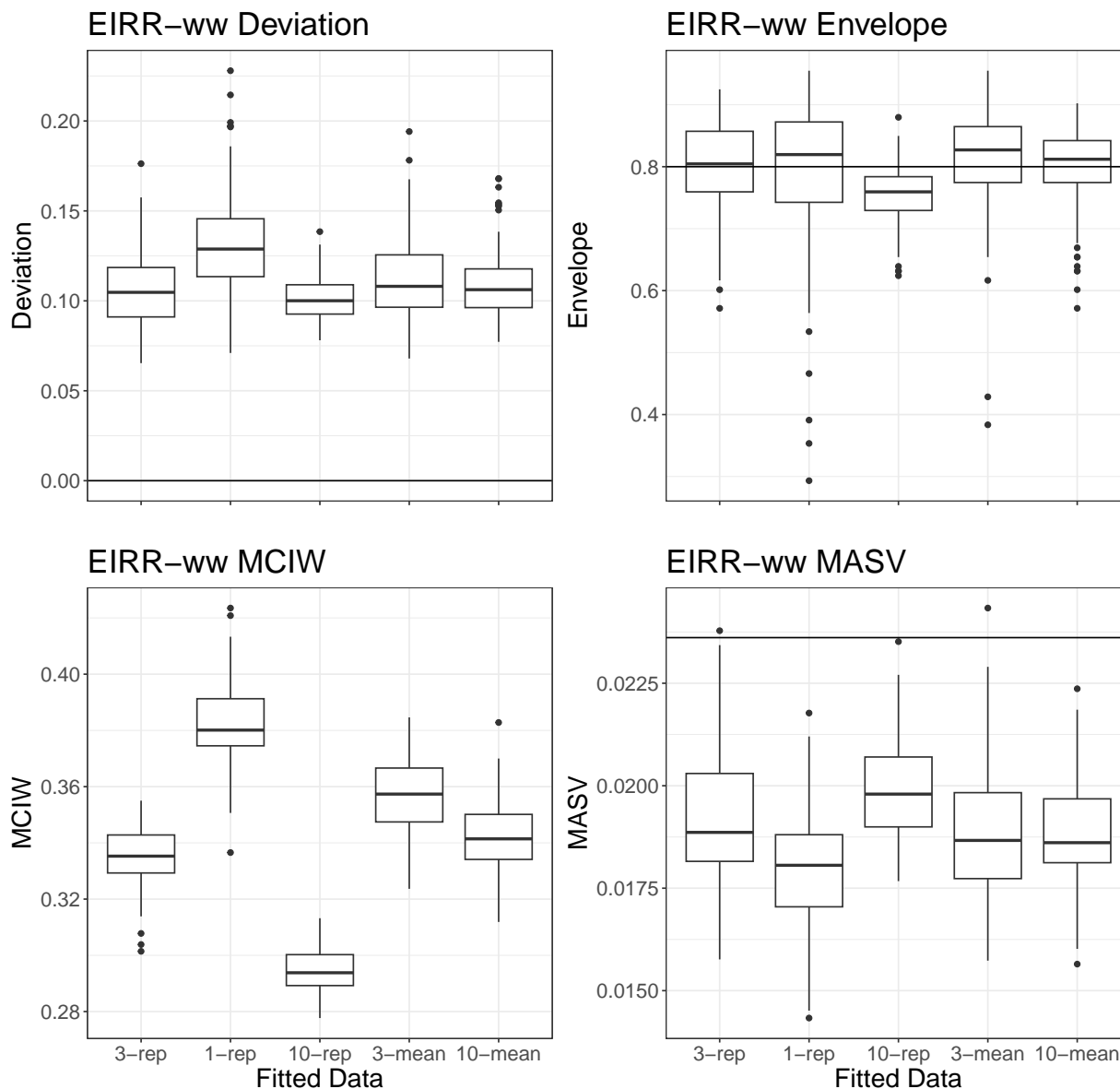


Figure 4: Frequentist metrics for performance of the EIRR-ww model using different kinds of wastewater data. The baseline scenario 3-reps uses three replicates, 1-rep uses one replicate, 10-reps uses ten replicates, 3-mean uses the mean of three replicates, 10-mean uses the mean of ten replicates. See Figure 3 for descriptions of the metrics.

3.3 Sensitivity analysis and comparison to state-of-the-art

We assessed the robustness of our model by changing the priors for the initial conditions, as well as the prior for λ . Frequentist metrics comparing these alternate models to the baseline

model are displayed in Figure A11. Changing these priors lead to only modest changes in model performance.

We fit the method by Huisman et al. [18] to each of our data sets, using as the input data the mean of three replicates. We then compared the Huisman et al. [18] method to the EIRR-ww model fit to three replicates. Also, the Huisman et al. method does not provide 80% credible intervals, so we compared metrics using 95% credible intervals. The comparison is visualized in Figure A12. In this simulation, the EIRR-ww model clearly outperforms the Huisman model in terms of both bias and precision associated with the effective reproduction number trajectory estimation.

3.4 Computational Considerations

The systems of ordinary differential equations for the EIR/EIRR models are linear, and thus can be solved in closed form. We used `Mathematica` Version (13.1) to calculate the closed form solution (see Appendix Section A.1.3). We conducted informal tests on a Macbook Air M2 (2022) to compare performance of using the EIRR-ww model with the closed form solution we derived vs the `Tsit5` solver [35] implemented in the `Julia` package `DifferentialEquations` [28]. First, we compared the EIRR-ww model fit to one realization of the baseline simulation scenario using the closed form solution versus the EIRR-ww model using the ODE solver. Next, we created a new data set using the same dynamics as the baseline scenario, but where wastewater data was sampled every twelve hours, so that the solution to the ODE system had to be solved every half-day as opposed to every day. The results of these experiments are displayed in Table A3. Although the computational benefit of using the closed form ODE solution is not substantial, not having to solve ODEs numerically has other advantages that we outline in the Discussion.

3.5 Estimating the effective reproduction number of SARS-CoV-2 in Los Angeles, CA

Wastewater data were collected from the Joint Water Pollution Control Plant (JWPCP), one of the largest wastewater treatment plants in Los Angeles County. The plant serves 4.8 million people across Los Angeles County. The data, reported as viral gene copies per ml of wastewater determined by quantitative PCR, were collected from the 24-hour composite wastewater influent samples at irregular, but approximately two-day intervals, and usually three replicates were reported for each sample [31]. We excluded two days (7/7/21 and 8/23/21) as outliers, as the reported concentrations dropped by at least two orders of magnitude compared to the concentrations of the closest previous and subsequent observed days. Cases during the same period in Los Angeles County are available from the California Open Data Portal [4]. The available data from cases and wastewater are visualized in Figure 5. Note that the two data sets are not perfectly comparable, as the cases are recorded for all of Los Angeles County, not just the population served by the JWPCP plant. We re-scaled the cases by a factor of 0.48 to partially account for this, as there are about 10 million people in Los Angeles County in total. Priors for the EIRR-ww and EIR-cases model were the same as those used in the simulation, except for the priors on the initial conditions and initial R_t (see Appendix Section A.2.7). For the Huisman et al. [18] method, we used the same shedding load profile calculated for the simulated data sets, but used the mean and standard deviation of the generation time distribution of SARS-CoV-2 calculated by Sender et al. [30]. The posterior estimate of R_t (from left to right) of the Huisman et al.

[18] method, the EIR-cases model and the EIRR-ww model are shown in Figure 6. For additional comparisons, we used two branching process models, the R_t -estim-gamma model fit to cases and total number of diagnostic tests [13] and another model fit to cases using the `epidemia` package [3, 29]. These are visualized along with the EIR-cases and EIRR-ww models in Figure A13.

While the EIRR-ww model provides different estimates than any of the case-based methods, they largely agree with each other in terms of estimating one large increase in R_t above 1 tied with the arrival of the Omicron variant in California in winter 2021. In contrast, the Huisman method estimates several dramatic changes in R_t over short spans of time, most notably an increase from below one to above 2 at the start of October 2021. Overall, we think the EIRR-ww model provides a better estimate of R_t than the Huisman method, both because it resembles estimates from other models using different data sources, and because it provides more epidemiologically plausible estimates than the Huisman method.

By incorporating the cumulative incidence compartment ($C(t)$) used in the EIR-cases model into the EIRR-ww model we are able to infer cumulative, and thus weekly, incidence using wastewater data. This allows us to estimate the time-varying posterior case detection rate by dividing the observed weekly case count by our posterior estimates of weekly incidence obtained from the EIRR-ww model. In addition, we calculate the case detection rate normalized by total diagnostic tests to account for changes in the case detection rate due to changes in available diagnostic tests. The posteriors are visualized in Figure A14. Both normalized and un-normalized versions of the estimated posterior case detection rate changed dramatically during the observation period. More details are available in Appendix Section A.2.9.

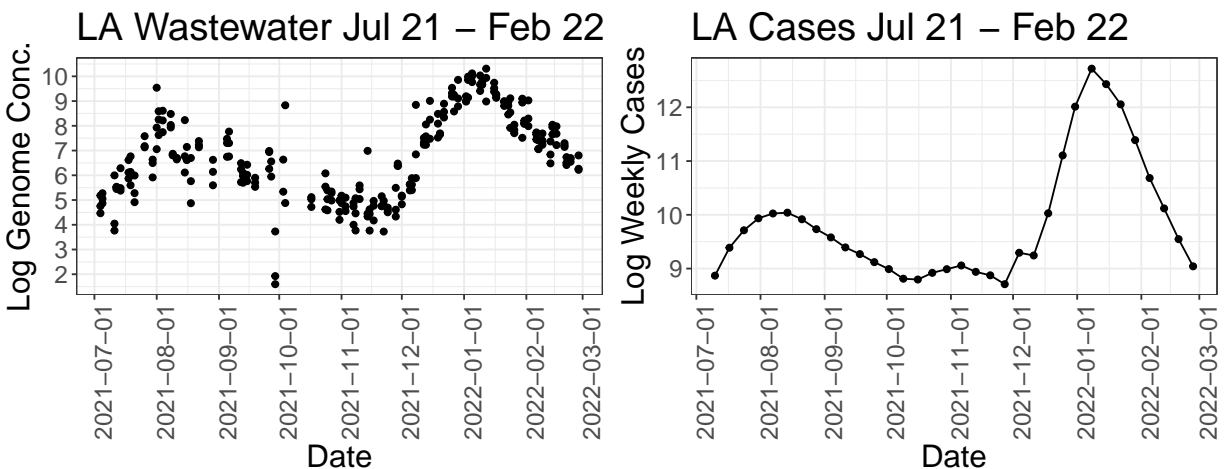


Figure 5: Wastewater and case data for the SARS-CoV-2 epidemic in Los Angeles, CA.

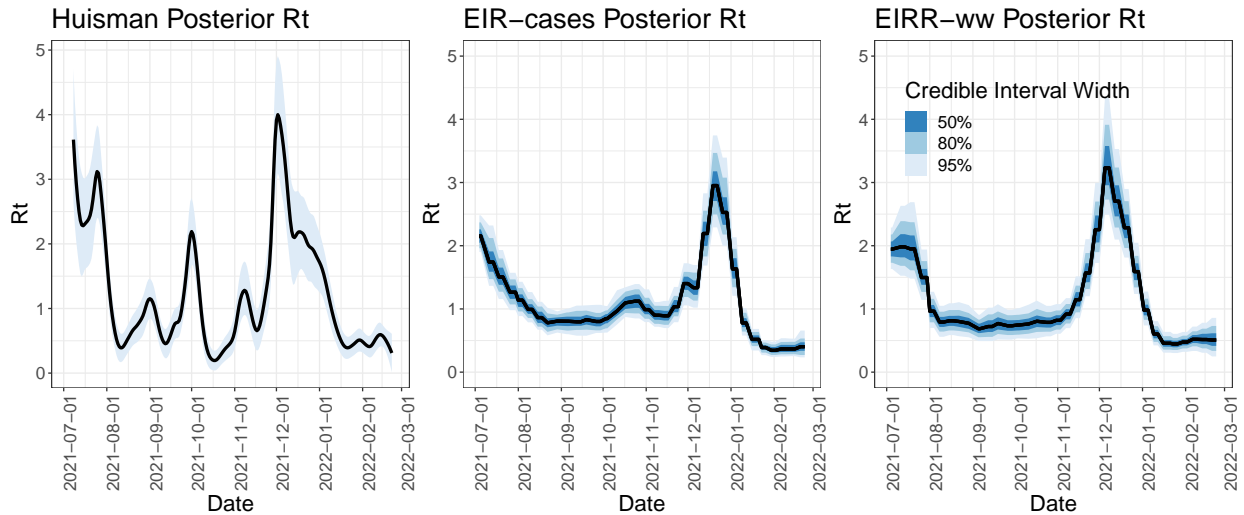


Figure 6: Posterior summaries of the effective reproduction number for the SARS-CoV-2 Delta and Omicron waves in Los Angeles, CA. Blue bars from dark to light represent 50, 80, and 95% credible intervals. Black lines represent median posterior estimates. EIRR-ww model and Huisman model are fit to RNA concentrations collected from wastewater data, EIR-cases model is fit to weekly case counts.

4 Discussion

We have presented a modeling framework for using simplified compartmental models coupled with Bayesian non-parametric priors to estimate the effective reproduction number. Using this framework, we created the EIRR-ww model to estimate the effective reproduction number using pathogen genome concentrations collected from wastewater samples. We tested the EIRR-ww model by fitting it to data simulated from an agent-based stochastic SEIRR model, and showed it could successfully estimate effective reproduction number dynamics. We also used the EIRR-ww model to estimate the effective reproduction number for SARS-CoV-2 in Los Angeles, California, showing it provides plausible estimates of the effective reproduction number when used on real world data.

When infected individuals shed pathogen genomes, they shed varying amounts of genomes depending on how long they have been infectious. It is not obvious that a compartmental model which does not account for these individual time-varying dynamics would be well equipped to handle such data. In fact, the SEIRR-ww model struggled to estimate the effective reproduction number on simulated data from our agent-based stochastic SEIRR model which explicitly modeled this time-varying property of genome shedding. In contrast, the EIRR-ww model had smaller bias and credible interval widths and was well calibrated from a frequentist perspective. In sensitivity analyses, we found these properties were relatively unchanged when priors that conflicted with the data were used. The gap in performance likely stems from the fact that both models use mis-specified observation models and the EIRR-ww model’s lack of an S compartment results in more flexibility for its estimates of the effective reproduction number, and thus better performance overall. The EIRR-ww model was unable to reconstruct the latent population compartments using only the linear relationship between compartment counts and concentrations (Figure A7), but reconstructed the trajectory well enough to provide good estimates of the effective reproduction number.

Our method clearly outperformed the Huisman et al. [18] method on both simulated and real data. We speculate the high levels of noise in both simulated and real data sets resulted in overly jagged estimates from `EpiEstim`, a problem we demonstrate directly in [13]. While the more detailed modeling approach of Nourbakhsh et al. [25] may yield better inference of the whole epidemic system when all assumptions are correct, it also may still produce biased estimates if the more detailed compartments still fail to account for the time-varying nature of pathogen shedding, as we saw with our SEIRR model in simulation. Our simpler model with fewer unverifiable assumptions is an appealing alternative when the main goal is effective reproduction number inference.

When compared to models fit to case data, the EIRR-ww model clearly had larger bias and wider credible intervals. This is likely the inevitable result of the high individual variation in genome concentrations seen in empirical studies [16], and an important limitation of this data source to keep in mind when considering using it in future models. On the other hand, in our simulation study we simulated the ideal scenario for cases, where the case detection rate does not change over time. In real world settings where this is likely not the case, models fit to wastewater data may outperform models fit to case data unless changes in reporting rates can be estimated by integrating multiple data sources (such as hospitalizations). Using models fit to both cases and wastewater data simultaneously seems like a promising direction for future work.

The EIR-cases model had slightly larger bias and wider credible intervals than the SEIR-cases model. However, this comparison was made when priors for the susceptible compartment were correct. In a real world situation where the initial susceptible population is hard to guess correctly, the EIR-cases model may well outperform the SEIR-cases model. Even in the best case scenario we showed in this paper, we think the increases in bias and uncertainty are acceptable. We did not use the SEIR-cases model to estimate R_t for Los Angeles, CA, in part because we think it is highly likely the rates of waning immunity changed dramatically when Omicron became the dominant SARS-CoV-2 variant. This is a situation for which the EIR framework is well suited, and indeed the estimates of R_t were largely in line with other case based methods. Even without wastewater data, we think the framework we describe in this paper is a useful alternative to `EpiEstim` and related methods when estimating the effective reproduction number.

Both the EIR and EIRR systems of ODEs are linear and thus have closed form solutions, which we used when implementing the models. For our particular application, we found this did not translate into substantial savings in computation time as compared to solving an ODE numerically, though we found the savings were larger when we increased the resolution of solutions needed from daily to half-daily. These results are likely algorithm and platform specific, as they depend heavily on how evaluation of ODE solutions, as well as ODE-based posterior gradients, are incorporated in the larger MCMC algorithm. Using an ODE solver inside an MCMC algorithm is a non-trivial undertaking, as tuning parameters controlling the tolerances for solver errors must be specified by the users [34]. Using the closed form solution, our informal testing suggests our computation times are at least as good as the ODE solver, and regardless of computation time, our method is more robust as it does not require properly specifying error tolerance tuning parameters.

We used both the EIRR-ww model as well as three other case based models to estimate the effective reproduction number of SARS-CoV-2 in Los Angeles, CA. We emphasize that all methods have their limitations, and so none should be taken as ground truth. However, the models agreed at many key points in time, including when R_t falls below one after the summer 2021 wave, and the general timing of the winter 2021 wave. This agreement suggests the

EIRR-ww model estimates are not unreasonable when fit to real data. An interesting point of disagreement is in the period from October 2021 to November 2021, when all three case models have a posterior median around one by the middle of October. In contrast, the EIRR-ww posterior median is well below one. One explanation for the discrepancy is that the case detection rate may have changed in October 2021. To explore this possibility, we estimated the case detection rate using posterior estimates of the incidence from the EIRR-ww model (Figure A14), which indeed show a sharp increase in the case detection rate (both the raw rate and the rate normalized by the total diagnostic tests) in October. These estimates should be viewed skeptically, as we found that in simulation, the EIRR-ww estimates for incidence were not particularly accurate (Figure A7). Still, we would expect the EIRR-ww model to perform worst at peaks, when the linearity assumption is particularly violated (the same counts of individuals shed different amounts of genomes if they are recently infected versus near the end of infectiousness, leading to different concentrations), so the change shown in our model estimates may still be real. When we examined the time series of hospitalizations from SARS-CoV-2 during this time period (Figure A15), a much more reliable data source than cases, it showed no sign of an increase in transmission rate in October (which we would expect to see reflected in an increase in hospitalizations in late October/early November). The other major point of disagreement is in July 2021, when the EIRR-ww model estimates R_t to be stable around 2 until August, while every case model estimates a steady decline in R_t . Here again the change in case detection rate may be to blame, but the hospitalizations are a little harder to interpret. The flatter hospitalization curve in August of 2021 may indicate the EIRR-ww model is correct, on the other hand, if R_t was indeed still at 2 on August 1st, we might expect a peak of hospitalizations even later than mid-August. We are inclined to think the case models are more correct in this case.

As a newly available data source, the best way to report wastewater data remains an open question. The number of replicates needed in order to conduct inference also remains an open question. In the United States, it is common practice to report averages of the replicates, for instance in the Nationwide Wastewater Monitoring Network and Wastewater-SCAN repositories [9, 38]. We focused instead on using replicates, and found that, when using simulated data, models using replicates performed modestly better than models relying on average concentrations. This suggests there is additional information available in the replicate concentrations, and it would be beneficial to report the replicates along with the averages. While the improvements in performance are not large, these improvements are basically free, costing only the time to change protocols for reporting data and the additional model run times of fitting models to larger data sets. We also found that using ten replicates instead of three produced only modestly improved model performance. Depending on the cost of producing replicates, increasing the number of replicates sampled may not be worth pursuing at this time.

An important limitation of our method is that it requires prior information concerning the dynamics of pathogen genome shedding, as well the temporal dynamics of the infection caused by the pathogen. In the case of SARS-CoV-2, the dynamics of pathogen RNA shedding have been studied, with the important caveat that all studies begin well after the point patients have been infected by the disease [16, 23, 2]. It is possible we are missing key information about the nature of pathogen shedding in the early stages of infection which would change our simulations and model. An ideal setting to collect this information would be a challenge trial, where individuals are deliberately infected with an infectious disease. To our knowledge, there has been one challenge trial of SARS-CoV-2 [19], but they do not report that any fecal matter was collected as part of the study. We would strongly

suggest future challenge trials collect samples of genomes shed through fecal matter, as these would provide invaluable information when developing statistical models for wastewater data. When applying wastewater data models to future emerging infectious diseases, it will be important to prioritize high quality studies of the temporal dynamics of pathogen shedding via fecal matter in order to make models such as ours useful.

We chose not to incorporate covariates that can control for changes in population size and conditions in the sewer system into our model. For our particular application, the JWPCP plant is so large, and collects wastewater from so many different smaller plants, that the population size and conditions are plausibly stable across time. In addition, there remains some controversy over exactly which covariates would be most useful to include [22]. Incorporating covariates which adjust for these changes is an important next step.

Acknowledgments

This work was in part funded by the UC Irvine Investing to Develop Center-Scale Multidisciplinary Convergence Research Programs Seed Funding Award and was made possible in part through support from the UC CDPH Modeling Consortium. DMP was supported by funding from the Bill & Melinda Gates Foundation (Award: INV-028123) and the NIAID (FAIN: U19AI089672). SCJ was supported by Water Research Foundation (WRF5093), U.S. National Science Foundation (CBET 2027306), University of California, Irvine Clinical Research Acceleration and Facilitation Team (CRAFT), and University of California, Irvine COVID-19 initiative. This work utilized the infrastructure for high-performance and high-throughput computing, research data storage and analysis, and scientific software tool integration built, operated, and updated by the Research Cyberinfrastructure Center (RCIC) at the University of California, Irvine. We thank the UC-CDPH modeling consortium, for useful discussion and feedback of intermediate work. Finally, we thank the Los Angeles County Sanitation Distribution for providing SARS-CoV-2 viral concentration data.

References

- [1] P. T. Acer, L. M. Kelly, A. A. Lover, and C. S. Butler. Quantifying the relationship between SARS-CoV-2 wastewater concentrations and building-level COVID-19 prevalence at an isolation residence: a passive sampling approach. *International Journal of Environmental Research and Public Health*, 19(18):11245, 2022.
- [2] A. E. Benefield, L. A. Skrip, A. Clement, R. A. Althouse, S. Chang, and B. M. Althouse. SARS-CoV-2 viral load peaks prior to symptom onset: a systematic review and individual-pooled analysis of coronavirus viral load from 66 studies. *medrxiv*, 2020.
- [3] S. Bhatt, N. Ferguson, S. Flaxman, A. Gandy, S. Mishra, and J. A. Scott. Semi-mechanistic Bayesian modeling of COVID-19 with renewal processes. *arXiv*, 2020. doi: 10.48550/ARXIV.2012.00394.
- [4] California Open Data Portal. California Open Data Portal. <https://data.ca.gov/dataset/covid-19-time-series-metrics-by-county-and-state1>, 2022. [Online; accessed 19-Jan-2022].

- [5] D. Champredon and J. Dushoff. Intrinsic and realized generation intervals in infectious-disease transmission. *Proceedings of the Royal Society B: Biological Sciences*, 282(1821): 2015–2026, 2015. doi: 10.1098/rspb.2015.2026.
- [6] D. Champredon, J. Dushoff, and D. J. D. Earn. Equivalence of the Erlang-Distributed SEIR Epidemic Model and the Renewal Equation. *SIAM Journal on Applied Mathematics*, 78(6):3258–3278, 2018. doi: 10.1137/18M1186411.
- [7] A. Cori, N. M. Ferguson, C. Fraser, and S. Cauchemez. A new framework and software to estimate time-varying reproduction numbers during epidemics. *American Journal of Epidemiology*, 178(9):1505–1512, 2013. doi: 10.1093/aje/kwt133.
- [8] Douglas Nychka, Reinhard Furrer, John Paige, and Stephan Sain. `fields`: Tools for spatial data, 2021. URL <https://github.com/dnychka/fieldsRPackage>. R package version 14.1.
- [9] C. Duvallet, F. Wu, K. A. McElroy, M. Imakaev, N. Endo, A. Xiao, J. Zhang, R. Floyd-O’Sullivan, M. M. Powell, S. Mendola, et al. Nationwide trends in COVID-19 cases and SARS-CoV-2 RNA wastewater concentrations in the United States. *ACS Es&t Water*, 2(11):1899–1909, 2022.
- [10] J. Friedman, R. Tibshirani, and T. Hastie. Regularization paths for generalized linear models via coordinate descent. *Journal of Statistical Software*, 33(1):1–22, 2010. doi: 10.18637/jss.v033.i01.
- [11] H. Ge, K. Xu, and Z. Ghahramani. Turing: A language for flexible probabilistic inference. In A. Storkey and F. Perez-Cruz, editors, *Proceedings of the Twenty-First International Conference on Artificial Intelligence and Statistics*, volume 84 of *Proceedings of Machine Learning Research*, pages 1682–1690. PMLR, 09–11 Apr 2018.
- [12] D. T. Gillespie. Exact stochastic simulation of coupled chemical reactions. *The Journal of Physical Chemistry*, 81(25):2340–2361, 1977.
- [13] I. H. Goldstein, J. Wakefield, and V. N. Minin. Incorporating testing volume into estimation of effective reproduction number dynamics. *arXiv preprint arXiv:2208.04418*, 2022.
- [14] M. S. Han, M.-W. Seong, N. Kim, S. Shin, S. Im Cho, H. Park, T. S. Kim, S. S. Park, and E. H. Choi. Viral RNA load in mildly symptomatic and asymptomatic children with COVID-19, Seoul, South Korea. *Emerging infectious diseases*, 26(10):2497, 2020.
- [15] M. D. Hoffman and A. Gelman. The No-U-Turn sampler: Adaptively setting path lengths in Hamiltonian Monte Carlo. *Journal of Machine Learning Research*, 15(47): 1593–1623, 2014.
- [16] T. Hoffmann and J. Alsing. Faecal shedding models for SARS-CoV-2 RNA among hospitalised patients and implications for wastewater-based epidemiology. *Journal of the Royal Statistical Society Series C: Applied Statistics*, 72(2):330–345, 2023.
- [17] J. S. Huisman, J. Scire, D. C. Angst, J. Li, R. A. Neher, M. H. Maathuis, S. Bonhoeffer, and T. Stadler. Estimation and worldwide monitoring of the effective reproductive number of SARS-CoV-2. *Elife*, 11:e71345, 2022.

- [18] J. S. Huisman, J. Scire, L. Caduff, X. Fernandez-Cassi, P. Ganesanandamoorthy, A. Kull, A. Scheidegger, E. Stachler, A. B. Boehm, B. Hughes, et al. Wastewater-based estimation of the effective reproductive number of SARS-CoV-2. *Environmental Health Perspectives*, 130(5):057011, 2022.
- [19] B. Killingley, A. J. Mann, M. Kalinova, A. Boyers, N. Goonawardane, J. Zhou, K. Lindsell, S. S. Hare, J. Brown, R. Frise, et al. Safety, tolerability and viral kinetics during sars-cov-2 human challenge in young adults. *Nature Medicine*, 28(5):1031–1041, 2022.
- [20] X. Li, H. H. Chang, Q. Cheng, P. A. Collender, T. Li, J. He, L. A. Waller, B. A. Lopman, and J. V. Remais. A spatial hierarchical model for integrating and bias-correcting data from passive and active disease surveillance systems. *Spatial and Spatio-Temporal Epidemiology*, 35:100341, 2020.
- [21] G. Lui, L. Ling, C. K. Lai, E. Y. Tso, K. S. Fung, V. Chan, T. H. Ho, F. Luk, Z. Chen, J. K. Ng, et al. Viral dynamics of SARS-CoV-2 across a spectrum of disease severity in COVID-19. *Journal of Infection*, 81(2):318–356, 2020.
- [22] R. Maal-Bared, Y. Qiu, Q. Li, T. Gao, S. E. Hrudey, S. Bhavanam, N. J. Ruecker, E. Ellehoj, B. E. Lee, and X. Pang. Does normalization of SARS-CoV-2 concentrations by Pepper Mild Mottle Virus improve correlations and lead time between wastewater surveillance and clinical data in Alberta (Canada): comparing twelve SARS-CoV-2 normalization approaches. *Science of The Total Environment*, 856:158964, 2023.
- [23] F. Miura, M. Kitajima, and R. Omori. Duration of SARS-CoV-2 viral shedding in faeces as a parameter for wastewater-based epidemiology: Re-analysis of patient data using a shedding dynamics model. *Science of The Total Environment*, 769:144549, 2021.
- [24] M. Morvan, A. L. Jacomo, C. Souque, M. J. Wade, T. Hoffmann, K. Pouwels, C. Lilley, A. C. Singer, J. Porter, N. P. Evens, et al. An analysis of 45 large-scale wastewater sites in England to estimate SARS-CoV-2 community prevalence. *Nature Communications*, 13(1):4313, 2022.
- [25] S. Nourbakhsh, A. Fazil, M. Li, C. S. Mangat, S. W. Peterson, J. Daigle, S. Langner, J. Shurgold, P. D’Aoust, R. Delatolla, et al. A wastewater-based epidemic model for SARS-CoV-2 with application to three Canadian cities. *Epidemics*, 39:100560, 2022.
- [26] Y. Okita, T. Morita, and A. Kumanogoh. Duration of SARS-CoV-2 RNA positivity from various specimens and clinical characteristics in patients with covid-19: a systematic review and meta-analysis. *Inflammation and Regeneration*, 42(1):1–19, 2022.
- [27] R Core Team. *R: A Language and Environment for Statistical Computing*. R Foundation for Statistical Computing, Vienna, Austria, 2023. URL <https://www.R-project.org/>.
- [28] C. Rackauckas and Q. Nie. Differentialequations.jl—a performant and feature-rich ecosystem for solving differential equations in julia. *Journal of Open Research Software*, 5(1):15, 2017.
- [29] J. A. Scott, A. Gandy, S. Mishra, S. Bhatt, S. Flaxman, H. J. T. Unwin, and J. Ish-Horowicz. Epidemia: An R package for semi-mechanistic Bayesian modelling of infectious diseases using point processes. *arXiv*, 2021. doi: 10.48550/ARXIV.2110.12461.

- [30] R. Sender, Y. Bar-On, S. W. Park, E. Noor, J. Dushoff, and R. Milo. The unmitigated profile of COVID-19 infectiousness. *Elife*, 11:e79134, 2022.
- [31] Z. Song, R. Reinke, M. Hoxsey, J. Jackson, E. Krikorian, N. Melitas, D. Rosso, and S. Jiang. Detection of SARS-CoV-2 in wastewater: Community variability, temporal dynamics, and genotype diversity. *Acs Es&T Water*, 1(8):1816–1825, 2021.
- [32] T. Stadler, D. Kühnert, S. Bonhoeffer, and A. J. Drummond. Birth–death skyline plot reveals temporal changes of epidemic spread in HIV and hepatitis C virus (HCV). *Proceedings of the National Academy of Sciences*, 110(1):228–233, 2013.
- [33] A. Svensson. A note on generation times in epidemic models. *Mathematical Biosciences*, 208(1):300–311, 2007.
- [34] J. Timonen, N. Siccha, B. Bales, H. Lähdesmäki, and A. Vehtari. An importance sampling approach for reliable and efficient inference in Bayesian ordinary differential equation models. *arXiv preprint arXiv:2205.09059*, 2022.
- [35] C. Tsitouras. Runge–Kutta pairs of order 5 (4) satisfying only the first column simplifying assumption. *Computers & Mathematics with Applications*, 62(2):770–775, 2011.
- [36] M. J. Wade, A. L. Jacomo, E. Armenise, M. R. Brown, J. T. Bunce, G. J. Cameron, Z. Fang, D. F. Gilpin, D. W. Graham, J. M. Grimsley, et al. Understanding and managing uncertainty and variability for wastewater monitoring beyond the pandemic: Lessons learned from the United Kingdom national COVID-19 surveillance programmes. *Journal of hazardous materials*, 424:127456, 2022.
- [37] K. A. Walsh, K. Jordan, B. Clyne, D. Rohde, L. Drummond, P. Byrne, S. Ahern, P. G. Carty, K. K. O’Brien, E. O’Murchu, et al. SARS-CoV-2 detection, viral load and infectivity over the course of an infection. *Journal of Infection*, 81(3):357–371, 2020.
- [38] WastewaterSCAN. WastewaterSCAN. <https://wastewaterscan.org>, 2023. [Online; accessed 9-May-2023].
- [39] R. Wölfel, V. M. Corman, W. Guggemos, M. Seilmaier, S. Zange, M. A. Müller, D. Niemeyer, T. C. Jones, P. Vollmar, C. Rothe, et al. Virological assessment of hospitalized patients with COVID-2019. *Nature*, 581(7809):465–469, 2020.
- [40] H. Xin, Y. Li, P. Wu, Z. Li, E. H. Lau, Y. Qin, L. Wang, B. J. Cowling, T. K. Tsang, and Z. Li. Estimating the latent period of coronavirus disease 2019 (COVID-19). *Clinical Infectious Diseases*, 74(9):1678–1681, 2022.
- [41] X. Xu, T. Kypraios, and P. D. O’Neill. Bayesian non-parametric inference for stochastic epidemic models using gaussian processes. *Biostatistics*, 17(4):619–633, 2016.
- [42] Q. Zhan, K. M. Babler, M. E. Sharkey, A. Amirali, C. C. Beaver, M. M. Boone, S. Comerford, D. Cooper, E. M. Cortizas, B. B. Currall, et al. Relationships between SARS-CoV-2 in wastewater and COVID-19 clinical cases and hospitalizations, with and without normalization against indicators of human waste. *Acs Es&T Water*, 2(11):1992–2003, 2022.

- [43] Y. Zhang, M. Cen, M. Hu, L. Du, W. Hu, J. J. Kim, and N. Dai. Prevalence and persistent shedding of fecal SARS-CoV-2 RNA in patients with COVID-19 infection: A systematic review and meta-analysis. *Clinical and Translational Gastroenterology*, 12(4), 2021.
- [44] A. Zulli, A. Pan, S. M. Bart, F. W. Crawford, E. H. Kaplan, M. Cartter, A. I. Ko, M. Sanchez, C. Brown, D. Cozens, et al. Predicting daily covid-19 case rates from SARS-CoV-2 RNA concentrations across a diversity of wastewater catchments. *FEMS microbes*, 2:xtab022, 2021.

A Appendix

A.1 Methods

A.1.1 Priors for models with the S compartment

We will assume the basic reproduction number is constant in a time interval $(k_i, k_{i+1}]$, defining it as $R_{0,k_i} = \frac{\beta_{k_i}}{\nu}$. Let M be the total number of time intervals of interest. Let $\mathbf{R}_0 = (R_{0,0}, R_{0,k_1}, \dots, R_{0,k_M})$, be the vector of basic reproduction numbers. We use a random walk prior so that

$$\begin{aligned} R_{0,0} &\sim \text{Log-Normal}(\mu_{0,0}, \sigma_{0,0}), \\ \sigma &\sim \text{Log-Normal}(\mu_{rw}, \sigma_{rw}), \\ \log(R_{0,k_{i+1}}) | \log(R_{0,k_i}), \sigma &\sim \text{Normal}(\log(R_{0,k_i}), \sigma_{rw}). \end{aligned}$$

For this study, we assume the basic reproduction number changes on a weekly basis, but it could change according to other time scales. Our model also requires initial conditions in order to solve the system of ODEs. Let N be the population size (assumed to be known). Let P be the population not in the $R2$ compartment at the time the model is fit. For simulations, this value is also known, in real world settings, we assume $N = P$, that is, the difference between the two is negligible in large populations. In the case of the SEIRR-wv model, the initial conditions are calculated as:

$$\begin{aligned} S(0) &= P * S_SEIR1, \\ I(0) &= (P - S(0)) * I_EIR1, \\ R1(0) &= (P - S(0) - I(0)) * R1_ER1, \\ E(0) &= (P - S(0) - I(0) - R1(0)), \\ R2(0) &= 1, \end{aligned}$$

where we define S_SEIR1 as the proportion of the population in the S compartment at time 0, I_EIR1 as the proportion of those in the E , I , or $R1$ compartments in the I compartment and $R1_ER1$ as the proportion of those in the E or $R1$ compartments in the $R1$ compartment. We use logit-normal priors for the proportions. We use a similar technique when using the SEIR-cases model, with one less parameter as there is only one R compartment.

A.1.2 Closed form solutions of the EIR/EIRR models

The systems of ordinary differential equations for the EIR/EIRR models are linear, and thus can be solved in closed form. We used `Mathematica` Version (13.1) to calculate the closed form solution (see the appendix for the solution to the EIRR ODE system).

A.1.3 Closed form solution for the EIRR Model

Define the EIRR model as:

$$\begin{aligned}\frac{dE}{dt} &= \alpha_t * I - \gamma E \\ \frac{dI}{dt} &= \gamma E - \nu I \\ \frac{dR1}{dt} &= \nu I - \eta R1 \\ \frac{dR2}{dt} &= \eta R1\end{aligned}$$

Let V be

$$V = \begin{bmatrix} -\gamma & \alpha_t & 0 & 0 \\ \gamma & -\nu & 0 & 0 \\ 0 & \nu & -\eta & 0 \\ 0 & 0 & \eta & 0 \end{bmatrix}.$$

The matrix exponential of V for a fixed α_t is reported on the next page. For initial conditions $M(t_0)$, the solution to the system of ODEs is

$$e^{V(t-t_0)}M(t_0).$$

$$a = 4\alpha\gamma + \gamma^2 - 2\gamma\nu + \nu^2$$

$$b = 3\eta + 3\gamma + 3\nu$$

$$c = -2\alpha\gamma + 2\eta\gamma + 2\eta\nu + 2\gamma\nu$$

$$A = \frac{\left(\frac{1}{2}(\alpha\gamma - \gamma(\eta - \gamma))(-\sqrt{a} - \gamma + \nu) + \gamma(\alpha(\eta - \nu) - \alpha\gamma)\right)e^{\frac{1}{2}t(-\sqrt{a} - \gamma - \nu)}}{\frac{1}{4}(-\sqrt{a} - \gamma - \nu)^2(b) + \frac{1}{2}(-\sqrt{a} - \gamma - \nu)(c) - \alpha\eta\gamma + \frac{1}{2}(-\sqrt{a} - \gamma - \nu)^3 + \eta\gamma\nu} + \frac{\left(\frac{1}{2}(\alpha\gamma - \gamma(\eta - \gamma))(\sqrt{a} - \gamma + \nu) + \gamma(\alpha(\eta - \nu) - \alpha\gamma)\right)e^{\frac{1}{2}t(\sqrt{a} - \gamma - \nu)}}{\frac{1}{4}(\sqrt{a} - \gamma - \nu)^2(b) + \frac{1}{2}(\sqrt{a} - \gamma - \nu)(c) - \alpha\eta\gamma + \frac{1}{2}(\sqrt{a} - \gamma - \nu)^3 + \eta\gamma\nu}$$

$$B = \frac{\left(\frac{1}{2}(-\sqrt{a} + \gamma - \nu)(\alpha(\eta - \nu) - \alpha\gamma) + \alpha(\alpha\gamma - \gamma(\eta - \gamma))\right)e^{\frac{1}{2}t(-\sqrt{a} - \gamma - \nu)}}{\frac{1}{4}(-\sqrt{a} - \gamma - \nu)^2(b) + \frac{1}{2}(-\sqrt{a} - \gamma - \nu)(c) - \alpha\eta\gamma + \frac{1}{2}(-\sqrt{a} - \gamma - \nu)^3 + \eta\gamma\nu} + \frac{\left(\frac{1}{2}(\sqrt{a} + \gamma - \nu)(\alpha(\eta - \nu) - \alpha\gamma) + \alpha(\alpha\gamma - \gamma(\eta - \gamma))\right)e^{\frac{1}{2}t(\sqrt{a} - \gamma - \nu)}}{\frac{1}{4}(\sqrt{a} - \gamma - \nu)^2(b) + \frac{1}{2}(\sqrt{a} - \gamma - \nu)(c) - \alpha\eta\gamma + \frac{1}{2}(\sqrt{a} - \gamma - \nu)^3 + \eta\gamma\nu}$$

$$C = \frac{\left(\frac{1}{2}(-\sqrt{a} - \gamma + \nu)(\gamma(\eta - \gamma) - \gamma\nu) + \gamma(\alpha\gamma - \nu(\eta - \nu))\right)e^{\frac{1}{2}t(-\sqrt{a} - \gamma - \nu)}}{\frac{1}{4}(-\sqrt{a} - \gamma - \nu)^2(b) + \frac{1}{2}(-\sqrt{a} - \gamma - \nu)(c) - \alpha\eta\gamma + \frac{1}{2}(-\sqrt{a} - \gamma - \nu)^3 + \eta\gamma\nu} + \frac{\left(\frac{1}{2}(\sqrt{a} - \gamma + \nu)(\gamma(\eta - \gamma) - \gamma\nu) + \gamma(\alpha\gamma - \nu(\eta - \nu))\right)e^{\frac{1}{2}t(\sqrt{a} - \gamma - \nu)}}{\frac{1}{4}(\sqrt{a} - \gamma - \nu)^2(b) + \frac{1}{2}(\sqrt{a} - \gamma - \nu)(c) - \alpha\eta\gamma + \frac{1}{2}(\sqrt{a} - \gamma - \nu)^3 + \eta\gamma\nu}$$

$$D = \frac{\left(\frac{1}{2}(-\sqrt{a} + \gamma - \nu)(\alpha\gamma - \nu(\eta - \nu)) + \alpha(\gamma(\eta - \gamma) - \gamma\nu)\right)e^{\frac{1}{2}t(-\sqrt{a} - \gamma - \nu)}}{\frac{1}{4}(-\sqrt{a} - \gamma - \nu)^2(b) + \frac{1}{2}(-\sqrt{a} - \gamma - \nu)(c) - \alpha\eta\gamma + \frac{1}{2}(-\sqrt{a} - \gamma - \nu)^3 + \eta\gamma\nu} + \frac{\left(\frac{1}{2}(\sqrt{a} + \gamma - \nu)(\alpha\gamma - \nu(\eta - \nu)) + \alpha(\gamma(\eta - \gamma) - \gamma\nu)\right)e^{\frac{1}{2}t(\sqrt{a} - \gamma - \nu)}}{\frac{1}{4}(\sqrt{a} - \gamma - \nu)^2(b) + \frac{1}{2}(\sqrt{a} - \gamma - \nu)(c) - \alpha\eta\gamma + \frac{1}{2}(\sqrt{a} - \gamma - \nu)^3 + \eta\gamma\nu}$$

$$E = \frac{\frac{\gamma\nu e^{-\eta t}}{-\alpha\gamma + \eta^2 - \eta\gamma - \eta\nu + \gamma\nu} + \frac{(-\gamma\nu\sqrt{a} + \gamma^2(-\nu) - \gamma\nu^2)e^{\frac{1}{2}t(-\sqrt{a} - \gamma - \nu)}}{2\left(\frac{1}{4}(-\sqrt{4\alpha\gamma + \gamma^2 - 2\gamma\nu + \nu^2} - \gamma - \nu)^2(b) + \frac{1}{2}(-\sqrt{a} - \gamma - \nu)(c) - \alpha\eta\gamma + \frac{1}{2}(-\sqrt{a} - \gamma - \nu)^3 + \eta\gamma\nu\right)} +$$

$$\frac{(\gamma\nu\sqrt{a} + \gamma^2(-\nu) - \gamma\nu^2)e^{\frac{1}{2}t(\sqrt{a} - \gamma - \nu)}}{2\left(\frac{1}{4}(\sqrt{a} - \gamma - \nu)^2(b) + \frac{1}{2}(\sqrt{a} - \gamma - \nu)(c) - \alpha\eta\gamma + \frac{1}{2}(\sqrt{a} - \gamma - \nu)^3 + \eta\gamma\nu\right)}$$

$$F = -\frac{e^{-\eta t}(\eta^2\nu - \eta\gamma\nu)}{\eta(-\alpha\gamma + \eta^2 - \eta\gamma - \eta\nu + \gamma\nu)} + \frac{(\nu^2\sqrt{a} + 2\alpha\gamma\nu - \gamma\nu^2 + \nu^3)e^{\frac{1}{2}t(-\sqrt{a} - \gamma - \nu)}}{2\left(\frac{1}{4}(-\sqrt{a} - \gamma - \nu)^2(b) + \frac{1}{2}(-\sqrt{a} - \gamma - \nu)(c) - \alpha\eta\gamma + \frac{1}{2}(-\sqrt{a} - \gamma - \nu)^3 + \eta\gamma\nu\right)} + \frac{(-\nu^2\sqrt{a} + 2\alpha\gamma\nu - \gamma\nu^2 + \nu^3)e^{\frac{1}{2}t(\sqrt{a} - \gamma - \nu)}}{2\left(\frac{1}{4}(\sqrt{a} - \gamma - \nu)^2(b) + \frac{1}{2}(\sqrt{a} - \gamma - \nu)(c) - \alpha\eta\gamma + \frac{1}{2}(\sqrt{a} - \gamma - \nu)^3 + \eta\gamma\nu\right)}$$

$$G = \frac{e^{-\eta t}(-\sqrt{a} + 2\eta - \gamma - \nu)(\sqrt{a} + 2\eta - \gamma - \nu)}{4(-\alpha\gamma + \eta^2 - \eta\gamma - \eta\nu + \gamma\nu)}$$

$$H = -\frac{\frac{\gamma\nu e^{-\eta t}}{-\alpha\gamma + \eta^2 - \eta\gamma - \eta\nu + \gamma\nu} + \frac{\eta\gamma\nu e^{\frac{1}{2}t(-\sqrt{a} - \gamma - \nu)}}{\frac{1}{4}(-\sqrt{a} - \gamma - \nu)^2(b) + \frac{1}{2}(-\sqrt{a} - \gamma - \nu)(c) - \alpha\eta\gamma + \frac{1}{2}(-\sqrt{a} - \gamma - \nu)^3 + \eta\gamma\nu} + \frac{\eta\gamma\nu e^{\frac{1}{2}t(\sqrt{a} - \gamma - \nu)}}{\frac{1}{4}(\sqrt{a} - \gamma - \nu)^2(b) + \frac{1}{2}(\sqrt{a} - \gamma - \nu)(c) - \alpha\eta\gamma + \frac{1}{2}(\sqrt{a} - \gamma - \nu)^3 + \eta\gamma\nu} +$$

$$I = \frac{\frac{\nu(\eta - \gamma)e^{-\eta t}}{-\alpha\gamma + \eta^2 - \eta\gamma - \eta\nu + \gamma\nu} - \frac{\eta\nu(\sqrt{a} - \gamma + \nu)e^{\frac{1}{2}t(-\sqrt{a} - \gamma - \nu)}}{2\left(\frac{1}{4}(-\sqrt{a} - \gamma - \nu)^2(b) + \frac{1}{2}(-\sqrt{a} - \gamma - \nu)(c) - \alpha\eta\gamma + \frac{1}{2}(-\sqrt{a} - \gamma - \nu)^3 + \eta\gamma\nu\right)} -$$

$$\frac{\eta\nu(-\sqrt{a} - \gamma + \nu)e^{\frac{1}{2}t(\sqrt{a} - \gamma - \nu)}}{2\left(\frac{1}{4}(\sqrt{a} - \gamma - \nu)^2(3\eta + 3\gamma + 3\nu) + \frac{1}{2}(\sqrt{a} - \gamma - \nu)(c) - \alpha\eta\gamma + \frac{1}{2}(\sqrt{a} - \gamma - \nu)^3 + \eta\gamma\nu\right)} + \frac{\eta\gamma\nu}{\eta\gamma\nu - \alpha\eta\gamma}$$

$$J = 1 - \frac{e^{-\eta t}(-\sqrt{a} + 2\eta - \gamma - \nu)(\sqrt{a} + 2\eta - \gamma - \nu)}{4(-\alpha\gamma + \eta^2 - \eta\gamma - \eta\nu + \gamma\nu)}$$

$$K = -\frac{\eta(\sqrt{a} - \gamma - \nu)(\sqrt{a} + \gamma + \nu)}{4(\eta\gamma\nu - \alpha\eta\gamma)}$$

$$e^V = \begin{pmatrix} A & B & 0 & 0 \\ C & D & 0 & 0 \\ E & F & G & 0 \\ H & I & J & K \end{pmatrix}$$

A.1.4 Branching process inspired models

For additional comparisons of our estimates of SARS-CoV-2 in Los Angeles, CA, we use two branching process inspired models that, unlike compartmental models, only model latent incidence. The Huisman et al. [18] method uses one example of this class of methods, but there are many others. The method relies on the so-called renewal equation which calculates current incidence as a product of a weighted sum of previous incidence and the effective reproduction number. Let I_t be the incidence at time t , R_t be the effective reproduction number at time t , and $g(t)$ be the probability density function of the generation time distribution (the time between an individual becoming infected and infecting another individual; under the compartmental model framework this is usually taken to be equivalent to the sum of the latent period and the infectious period [33, 5, 6]). Then the classic renewal equation is:

$$E[I_t | I_1, \dots, I_{t-1}] = R_t \sum_{s=1}^{t-1} I_s g(t-s).$$

The `epidemia` package can be used to create different branching process inspired models to estimate the effective reproduction number using different observation models and models for latent incidence [29]. For the model we used in this study, we modeled observed cases using a negative binomial distribution, modeled the effective reproduction number as a Gaussian random walk, and modeled unobserved incidence as an auto-regressive normal random variable with variance equal to the mean multiplied by an over-dispersion parameter. The explicit model is listed below:

$$\begin{aligned} \tau &\sim \exp(\lambda)\text{-Hyperprior for unobserved incidence,} \\ I_\nu &\sim \exp(\tau)\text{-Prior on unobserved incidence } \nu \text{ days before observation,} \\ I_{\nu+1}, \dots, I_0 &= I_\nu\text{-Unobserved incidence,} \\ \sigma &\sim \text{Truncated-Normal}(0, 0.1^2)\text{-Prior on variance of random walk} \\ \log R_0 &\sim \text{Normal}(\log 2, 0.2^2)\text{-Prior on } R_0, \\ \log R_t | \log R_{t-1} &\sim \text{Normal}(\log R_{t-1}, \sigma)\text{-Random walk prior on } R_t, \\ \psi &\sim \text{Normal}(10, 2)\text{-Prior on variance parameter for incidence,} \\ I_t | I_\nu, \dots, I_{t-1} &\sim \text{Normal}\left(R_t \sum_{s<t} I_s g_{t-s}, \psi\right)\text{-Model for incidence,} \\ \alpha &\sim \text{Normal}(0.13, 0.7^2)\text{-Prior on case detection rate,} \\ y_t &= \alpha_t \sum_{s<t} I_s \pi_{t-s}\text{-Mean of observed data model,} \\ \phi &\sim P(\phi)\text{-Prior on dispersion parameter for observed data,} \\ Y_t &\sim \text{Neg-Binom}(y_t, \phi)\text{-Observed data model.} \end{aligned}$$

Here π_t are the values of the probability density function for the delay distribution, the time between an individual being infected and being observed. We also used the Rt-estim-gamma model, which is similar to the model above, but uses total diagnostic tests as a model covariate in the observation model. This allows the rate of detection to change over time as a function of available tests, avoiding the situation, for example, where an increase in cases due to test availability is mistaken for an increase in cases due to increased incidence. Full details are available in [13].

A.2 Results

A.2.1 Simulating an agent-based stochastic SEIRR model

An agent stochastic SEIRR model is an N -dimensional continuous time Markov chain, where N is the population. The state-space is then $\{S, E, I, R1, R2\}^N$. When represented as a vector $G(t)$, each entry of $G(t)$ records the state of one of the N individuals, i.e. if the i th entry of $G(t)$, $G(t)_i$ is S , then the i th individual is susceptible at time t . Let $I(t)$ be the number of infectious individuals at time t . It can be defined in terms of its transition rates from state G to state G' so that

$$\lambda_{GG'} = \begin{cases} \beta_t/N \times I(t) & \text{if } G_j = S \text{ and } G'_j = E \\ \gamma & \text{if } G_j = E \text{ and } G'_j = I \\ \nu & \text{if } G_j = I \text{ and } G'_j = R1 \\ \eta & \text{if } G_j = R1 \text{ and } G'_j = R2 \\ 0 & \text{otherwise} \end{cases}$$

The well known Gillespie algorithm popularized in [12] can be used to simulate from this model, but it is quite slow. We employ a variation of the Gillespie algorithm in order to simulate individuals and their individual state transition times. In essence, as an individual enters the simulation (via infection) all future transition times for that individual are simulated at once. Then, the next event is simply the most recent transition time amongst all individuals still in the simulation. In pseudocode, the basic algorithm is

Algorithm 1 Individual Gillespie Algorithm

```
 $i \leftarrow$  initial I  
 $e \leftarrow$  initial E  
 $r1 \leftarrow 0$   
 $s \leftarrow N - i - e$   
 $t_i \leftarrow$  Initial infectious times  
 $t_{r1} \leftarrow$  Initial recover times  
 $t_{r2} \leftarrow$  Initial stop shedding times  
 $t \leftarrow \max t_i$   
while  $i > 0 | r1 > 0$  do  
  if  $s > 0 \& i > 0$  then  
     $n_e \leftarrow t + \text{Exp}(\beta \times s \times i)$   
  else if  $s = 0 | i = 0$  then  
     $n_e \leftarrow \text{inf}$   
  end if  
   $n_i \leftarrow \min t_i$   
   $n_{r1} \leftarrow \min t_{r1}$   
   $n_{r2} \leftarrow \min t_{r2}$   
   $n_t \leftarrow \min n_e, n_i, n_{r1}, n_{r2}$   
   $t \leftarrow n_t$   
  if  $n_t = n_e$  then  
     $s \leftarrow s - 1$   
     $e \leftarrow e + 1$   
     $x \sim \text{Exp}(\gamma)$   
     $y \sim \text{Exp}(\nu)$   
     $z \sim \text{Exp}(\eta)$   
     $t_i \leftarrow \text{append}(t_i, t + x)$   
     $t_{r1} \leftarrow \text{append}(t_{r1}, t + x + y)$   
     $t_{r2} \leftarrow \text{append}(t_{r2}, t + x + y + z)$   
  else if  $n_t = n_i$  then  
     $e \leftarrow e - 1$   
     $i \leftarrow i + 1$   
     $t_i \leftarrow \text{remove}(t_i, n_i)$   
  else if  $n_t = n_{r1}$  then  
     $i \leftarrow i - 1$   
     $r1 \leftarrow r1 + 1$   
     $t_{r1} \leftarrow \text{remove}(t_{r1}, n_{r1})$   
  else if  $n_t = n_{r2}$  then  
     $r1 \leftarrow r1 - 1$   
     $t_{r2} \leftarrow \text{remove}(t_{r2}, n_{r2})$   
  end if  
end while
```

We omit the various pieces of code which ensure that all of the individual transition times are recorded and associated with the correct individuals. It is easy to adapt this algorithm to allow for a changing β at known change point times. We simply add an additional check, where the next event can be any of the nearest future transition times, or the nearest future change point time. We use this adapted version when we simulate data to test the EIRR-

ww model. In order to calculate individual genome concentrations, we use the consensus shedding profile for SARS-CoV-2 RNA created by Nourbakhsh et al. [25]. We manually recorded the values displayed in the figure, and then used a thin plate regression spline (using the R package `fields` [8]) to create a continuous curve. The spline fit and manually recorded values are displayed in Figure A1.

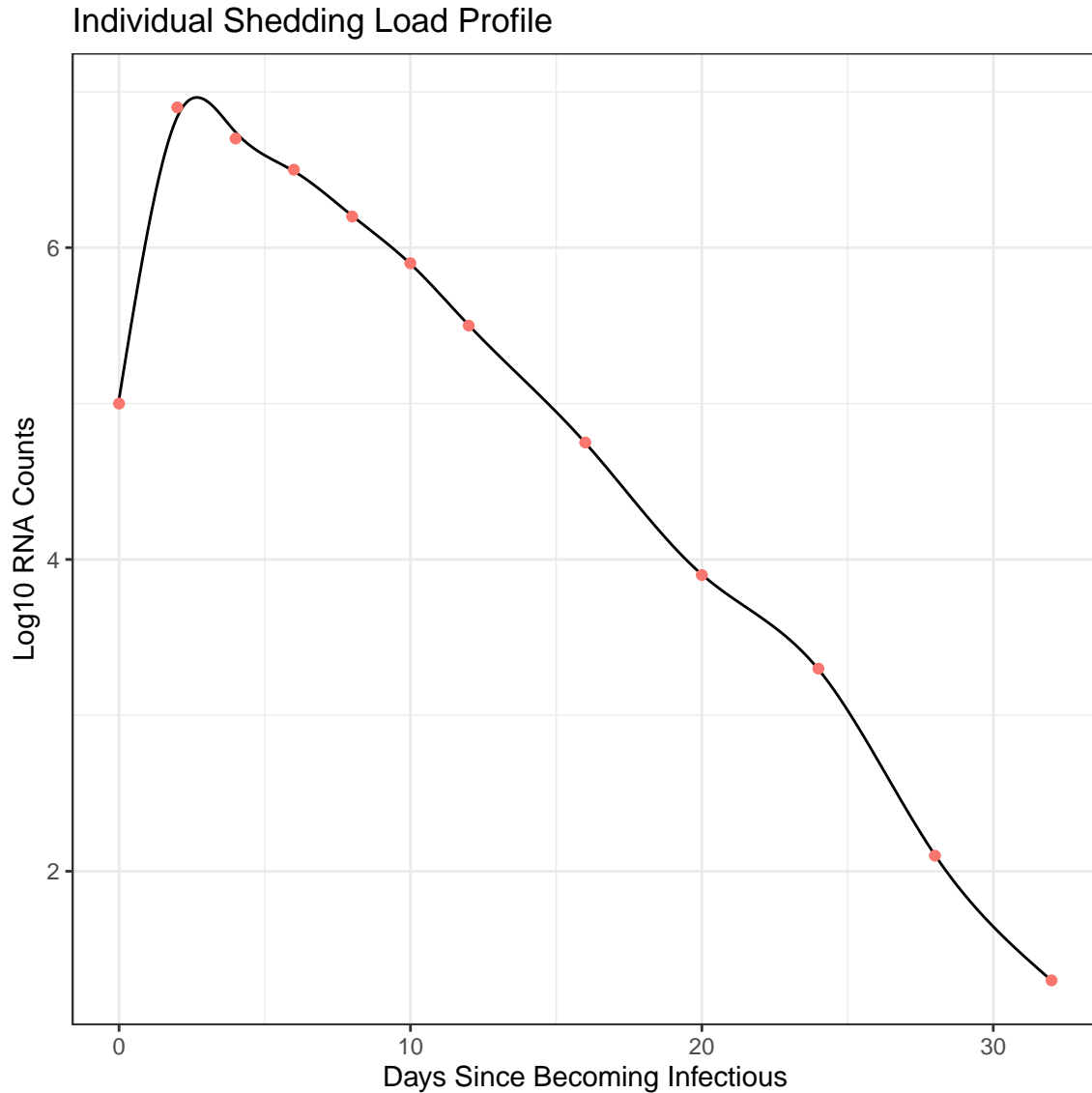


Figure A1: Thin plate spline fit to manually recorded values from the consensus shedding load profile developed by Nourbakhsh et al. (2022). Red dots are the manually recorded values. Black line is the spline fit.

To calculate the mean log genome concentration shed by an individual at time l , we first checked to see if they were in the I or $R1$ compartments at time l , then predicted mean log genome concentration using the fitted spline and the difference between l and the time they became infectious.

A.2.2 Comparing Simulation Engines

We compare our variation on the Gillespie algorithm to both a traditional Agent based model (Agent) and a compartmental model (Compartment) simulated using the traditional Gillespie algorithm. We set the population to be 100, set R_0 to 1.5 and initialized with 5 infectious individuals and all other individuals in the susceptible population. We simulated 10000 simulations from each of the three engines, and plotted the mean and quantiles of the counts in each of the compartments in the first 100 days. For the agent and variation models, we also plotted the log concentrations on each of the first 100 days. We see no evidence the three engines are not equivalent.

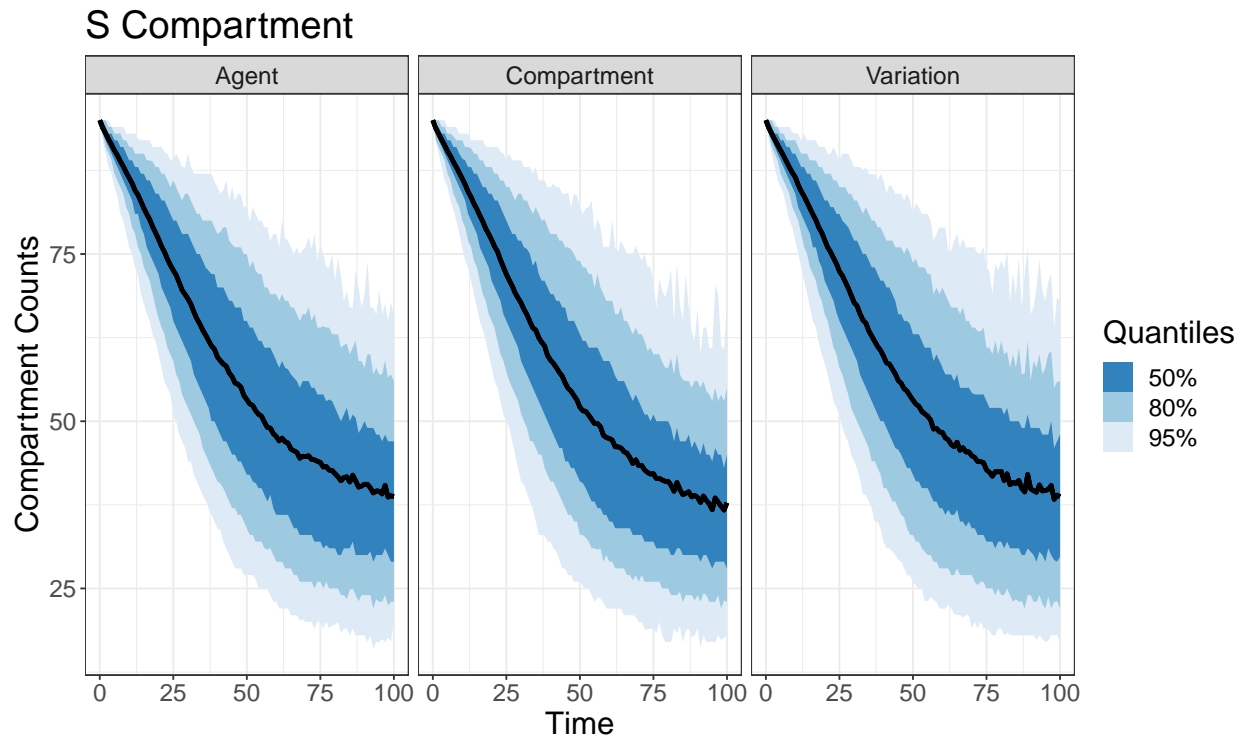


Figure A2: Counts in the S compartment across three simulation engines. Blue bars are quantiles, black lines are means.

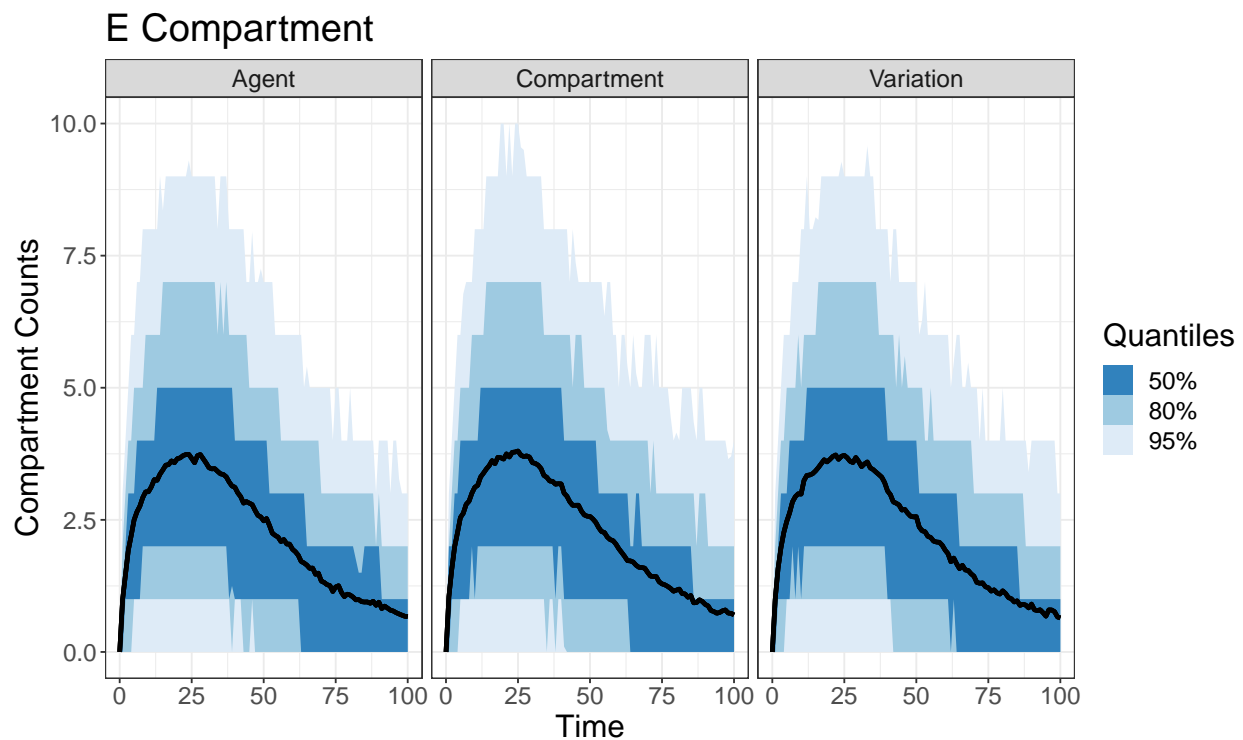


Figure A3: Counts in the E compartment across three simulation engines. Blue bars are quantiles, black lines are means.

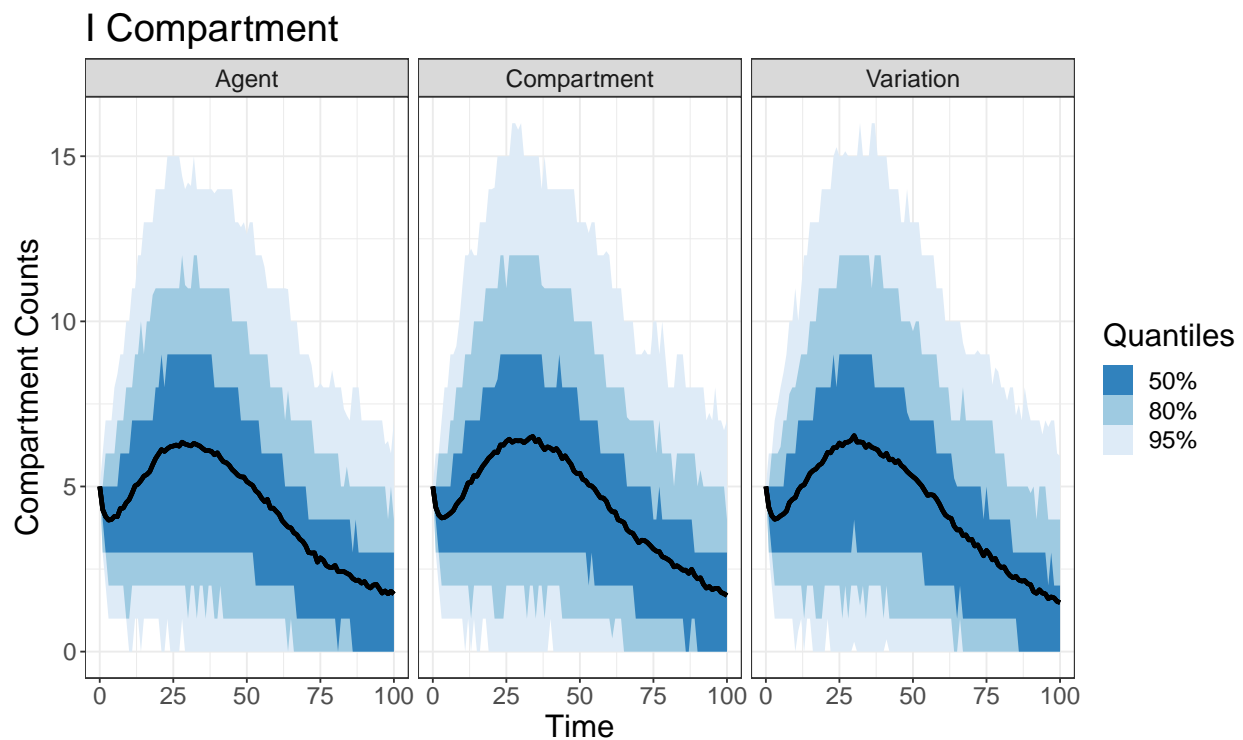


Figure A4: Counts in the I compartment across three simulation engines. Blue bars are quantiles, black lines are means.

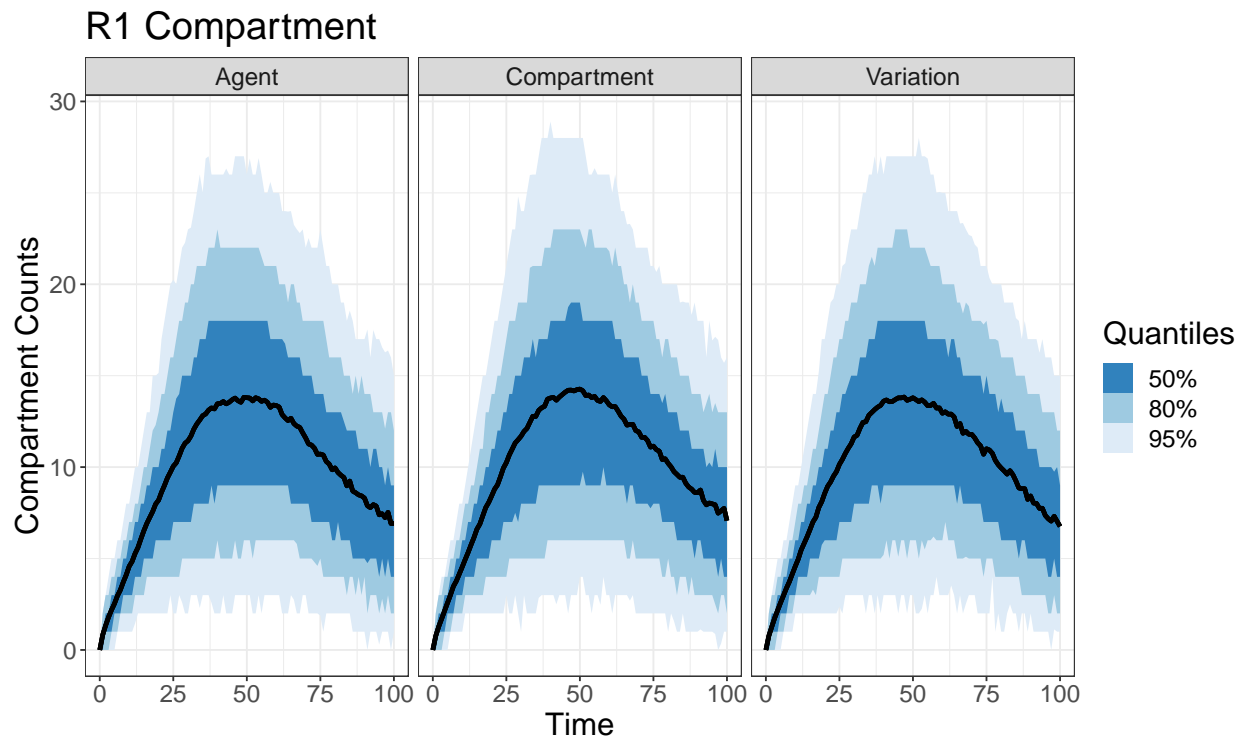


Figure A5: Counts in the R1 compartment across three simulation engines. Blue bars are quantiles, black lines are means.

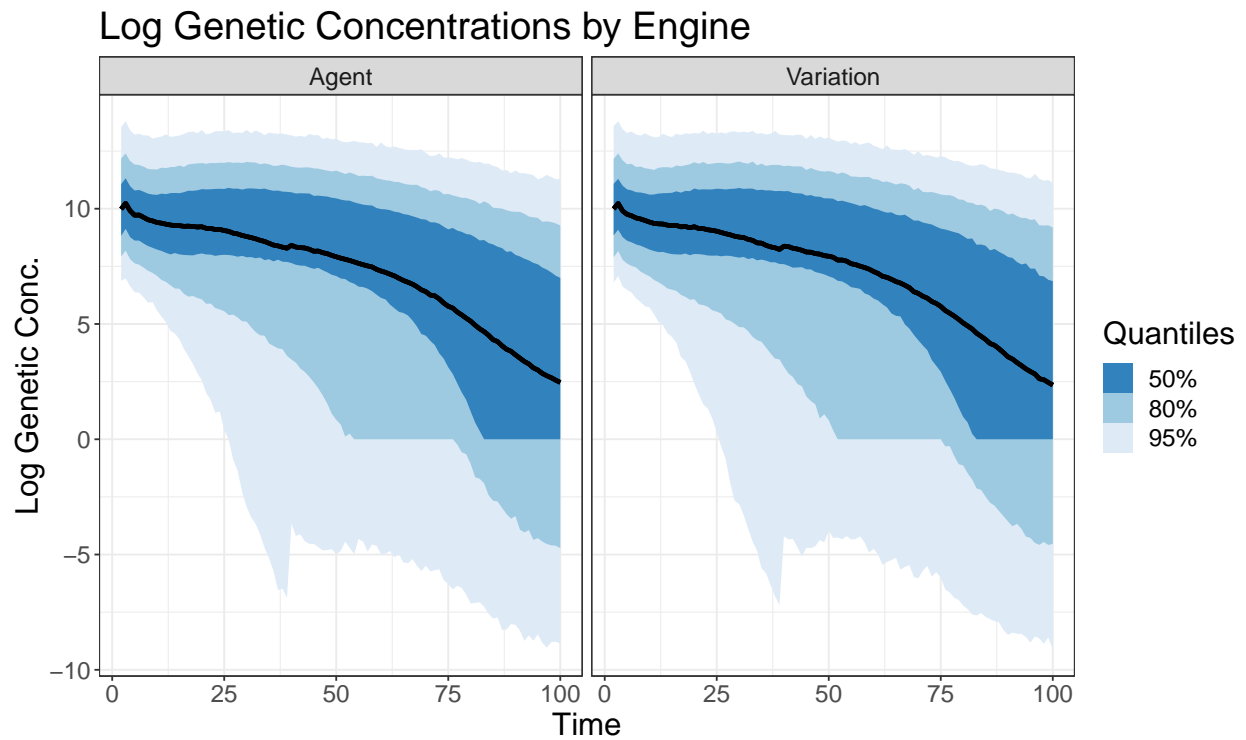


Figure A6: Simulated log concentrations across two simulation engines. Blue bars are quantiles, black lines are means.

A.2.3 Simulation parameters

For choosing the prior for λ , the population was 1000, R_0 was set to 2, and the parameters for γ , ν and η were drawn from the priors in Table A2. Five individuals were initially in the I compartment, the other individuals were in the S compartment.

The parameters used for the simulation producing observed data used in the simulation studies described in the main text are displayed below. The population size was 100000, the model was initialized with 200 individuals in the E compartment and 200 in the I compartment, all others were in the S compartment. The basic reproduction number was set to 1.75 for five weeks, 0.7 for four weeks, and then increased from 0.7 to 0.9 for two weeks before following the trajectory chosen for the observed data period.

Parameter	Interpretation	Value
$1/\gamma$	Mean latent period duration	4
$1/\nu$	Mean infectious period duration	7
$1/\eta$	Mean duration when recovered but still shedding RNA	18
ρ	scales concentrations of RNA into observed concentrations	0.011
τ	describes the noisiness of observed gene data	0.5

Table A1: Simulation parameters used in the simulation study. Durations are measured in days.

The estimate for $1/\gamma$ was calculated by averaging the mean latent period calculated by Xin et al. [40] with the mean time to detecting virus which could be cultured found in [19]. We took culturable virus to be a proxy for infectiousness. The mean time from infectiousness to symptom onset was 1.37, calculated again as an average from the previous two studies (1.4 days from [40] versus 1.33 from [19]). Mean infectious period was calculated using the mean period of detecting virus which could be cultured found in [19]. Many studies have calculated the time from symptom onset to the end of RNA shedding in fecal matter; we averaged the estimates from [26] and [43]. Because these two literature reviews shared studies, we disaggregated their estimates into individual study estimates, counting each study only once in our final average. We used mean shedding estimates from each study reported by Okita et al. [26]. Zhang et al. [43] did not include estimates of the mean for each study in their review, if estimates of the mean duration were available from the original paper, they were used, if they were not, the paper was not included in the final average. We also examined the literature review by Walsh et al. [37], but found no new studies with more than two samples not in the previous two reviews. We decided to exclude studies with fewer than three samples. The final average duration from symptom onset to the end of RNA shedding in fecal matter was 22.99 days. We calculated $1/\eta$ (the mean duration of shedding after recovery) as

$$1/\eta = 22.99 + 1.33 - 1/\nu = 17.86.$$

Note we are assuming shedding begins at the start of the infectious period. To calculate a plausible τ (standard deviation from true genetic concentration), we used the JWPCP data, and fit a Bayesian thin plate regression generalized student t-distribution spline to the data. We used the mean of the posterior estimate of τ for the τ in our simulation. The value for ρ (scaling factor for the mean of the generalized t-distribution) was chosen arbitrarily so that the mean total genome concentrations produced by the simulation would be roughly similar to the means seen in the JWPCP data. Note that all of the parameters are based on studies of the original Wuhan lineage of SARS-CoV-2.

Table A2: Priors used by all models in the baseline simulation scenario.

Parameter	Model	Prior	Prior Median (95% Interval)	Truth
γ	All	Log-normal($\log(1/4)$, 0.2)	0.25 (0.17, 0.37)	0.25
ν	All	Log-normal($\log(1/7)$, 0.2)	0.14 (0.10, 0.21)	0.14
σ_{rw}	All	Log-normal($\log(0.1)$, 0.2)	0.1 (0.07, 0.15)	NA
η	SEIRR-ww/EIRR-ww	Log-normal($\log(1/18)$, 0.2)	0.06 (0.04, 0.08)	0.06
$R_{0,0}$	SEIRR-ww/SEIR-cases	Log-Normal($\log(0.88)$, 0.1)	0.88 (0.72, 1.07)	0.9
λ	SEIRR-ww/EIRR-ww	Logit-normal(5.69, 2.18)	0.997 (0.81, 1)	NA
τ	SEIRR-ww/EIRR-ww	Log-normal(0, 1)	1.00 (0.14, 7.10)	0.5
df	SEIRR-ww/EIRR-ww	Gamma(10,2)	19.33 (9.59, 34.17)	2.99
ρ	SEIRR-ww/EIRR-ww	Log-normal(0, 1)	1.00 (0.14, 7.10)	NA
R_0	EIRR-ww/EIR-cases	Log-Normal($\log(0.88)$, 0.1)	0.88 (0.72, 1.07)	0.80
ψ	SEIR-cases/EIR-cases	Logit-Normal(-1.39, 0.4)	0.20 (0.10, 0.35)	0.2
ϕ	SEIR-cases/EIR-cases	Log-Normal(4.22, 0.29)	68.03 (38.54, 120.11)	57.55
S_SEIR1	SEIRR-ww	Logit-Normal(3.47, 0.05)	0.97 (0.967, 0.972)	0.97
I_EIR1	SEIRR-ww	Logit-Normal(-1.548302, 0.05)	0.18 (0.16, 0.19)	0.18
$R1_ER1$	SEIRR-ww	Logit-Normal(2.22, 0.05)	0.90 (0.89, 0.91)	0.90
S_EI	SEIR-cases	Logit-Normal(4.83, 0.05)	0.992 (0.991, 0.993)	0.992
I_EI	SEIR-cases	Logit-Normal(0.78, 0.05)	0.68 (0.66, 0.71)	0.68
$E(0)$	EIRR-ww/EIR-cases	Normal(225, 0.05)	225.00 (224.90, 225.01)	225
$I(0)$	EIRR-ww/EIR-cases	Normal(489, 0.05)	489.00 (448.90, 489.01)	489
$R1(0)$	EIRR-ww	Normal(2075, 0.05)	2075.00 (2074.90, 2075.01)	2075

A.2.4 EIRR-ww model performance in scenario 1

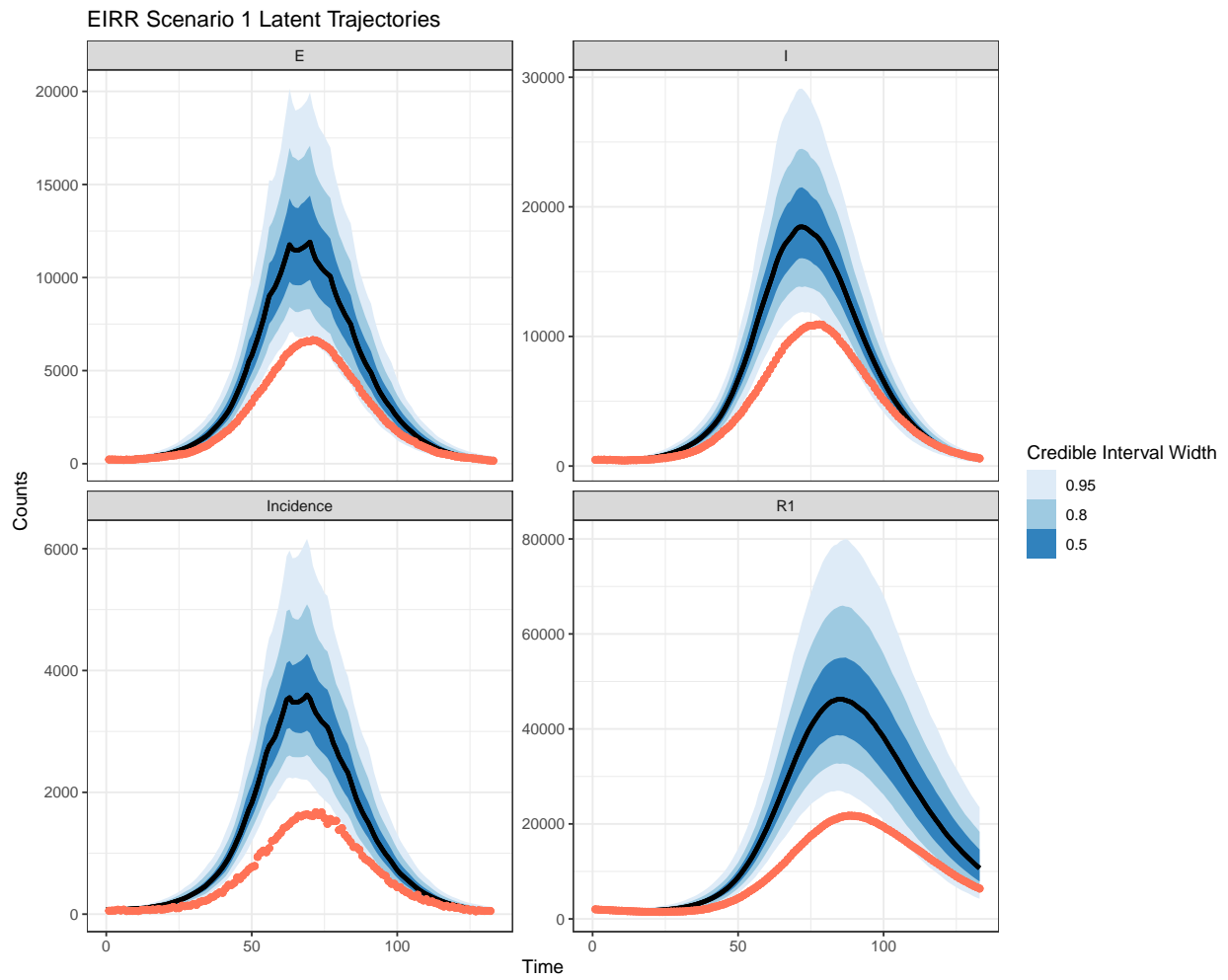


Figure A7: EIRR-ww posterior summaries for latent unobserved compartments and incidence. Posterior is from the model fit shown in Figure 2. Blue bars are credible intervals, black lines are medians, true values are shown in red.

EIRR Scenario 1 Fixed Parameters

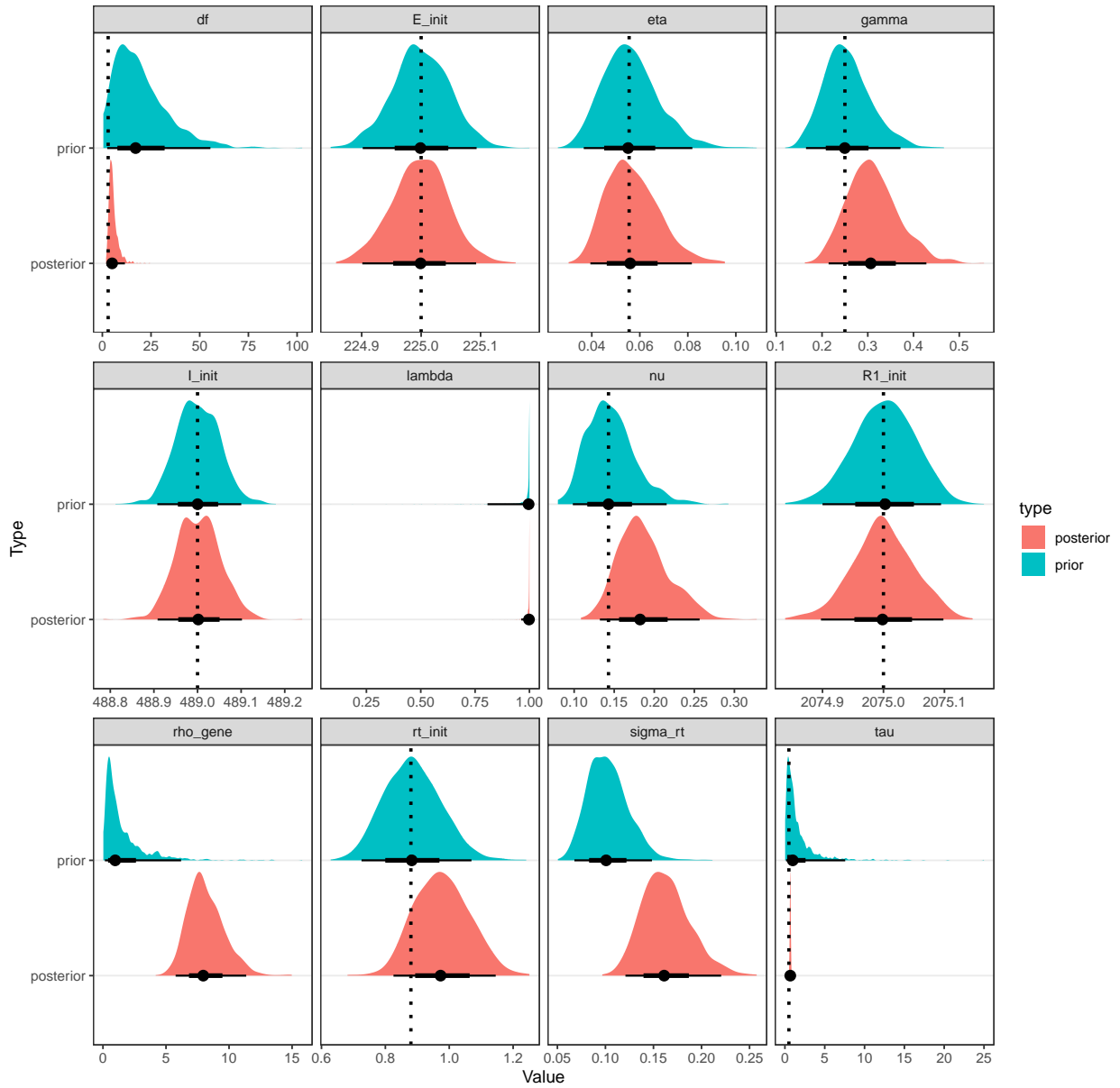


Figure A8: EIRR-ww prior and posterior summaries for fixed model parameters. Posterior summaries are from the model fit shown in Figure 2. Blue densities are the prior, red densities are the posterior, dotted lines indicate true values (when relevant).

EIRR Scenario 1 Posterior Predictive

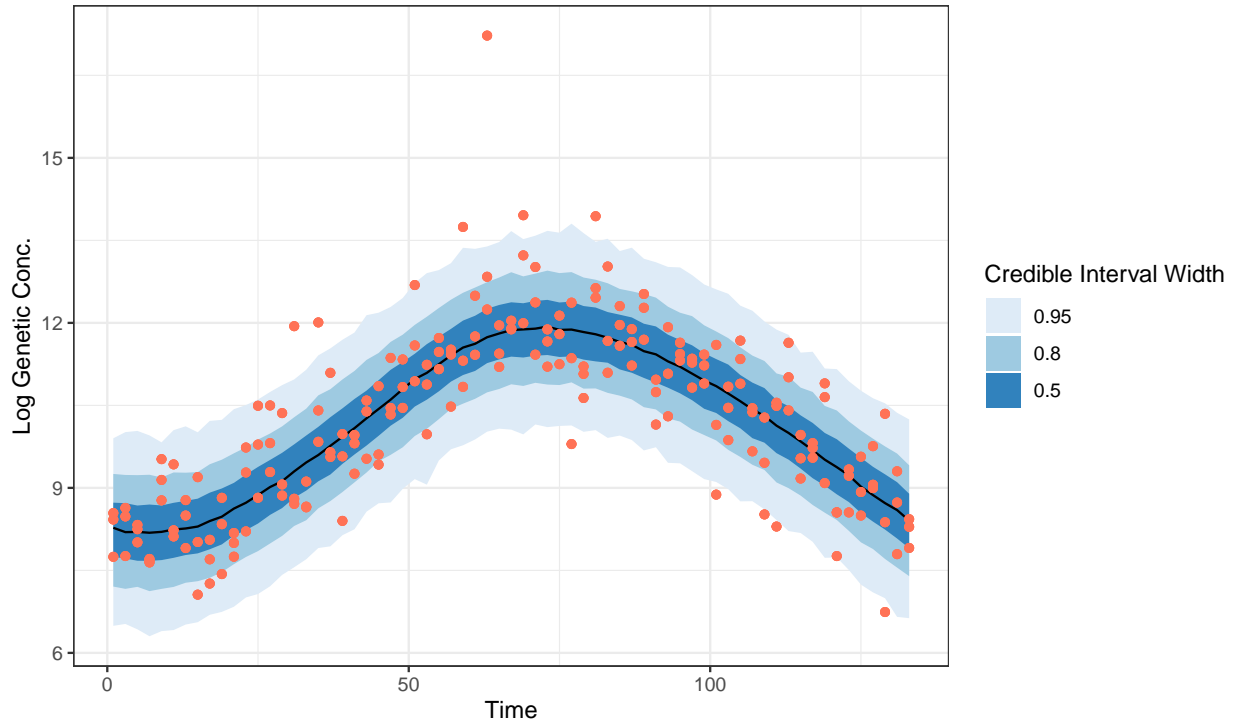


Figure A9: EIRR-ww posterior predictive of Log genome concentrations. Posterior predictive summaries are from the model fit shown in Figure 2. Blue bars represent credible intervals, black lines medians, and red dots are observed data.

A.2.5 Additional Simulation Results

Frequentist Metrics Across Models (95% CI)

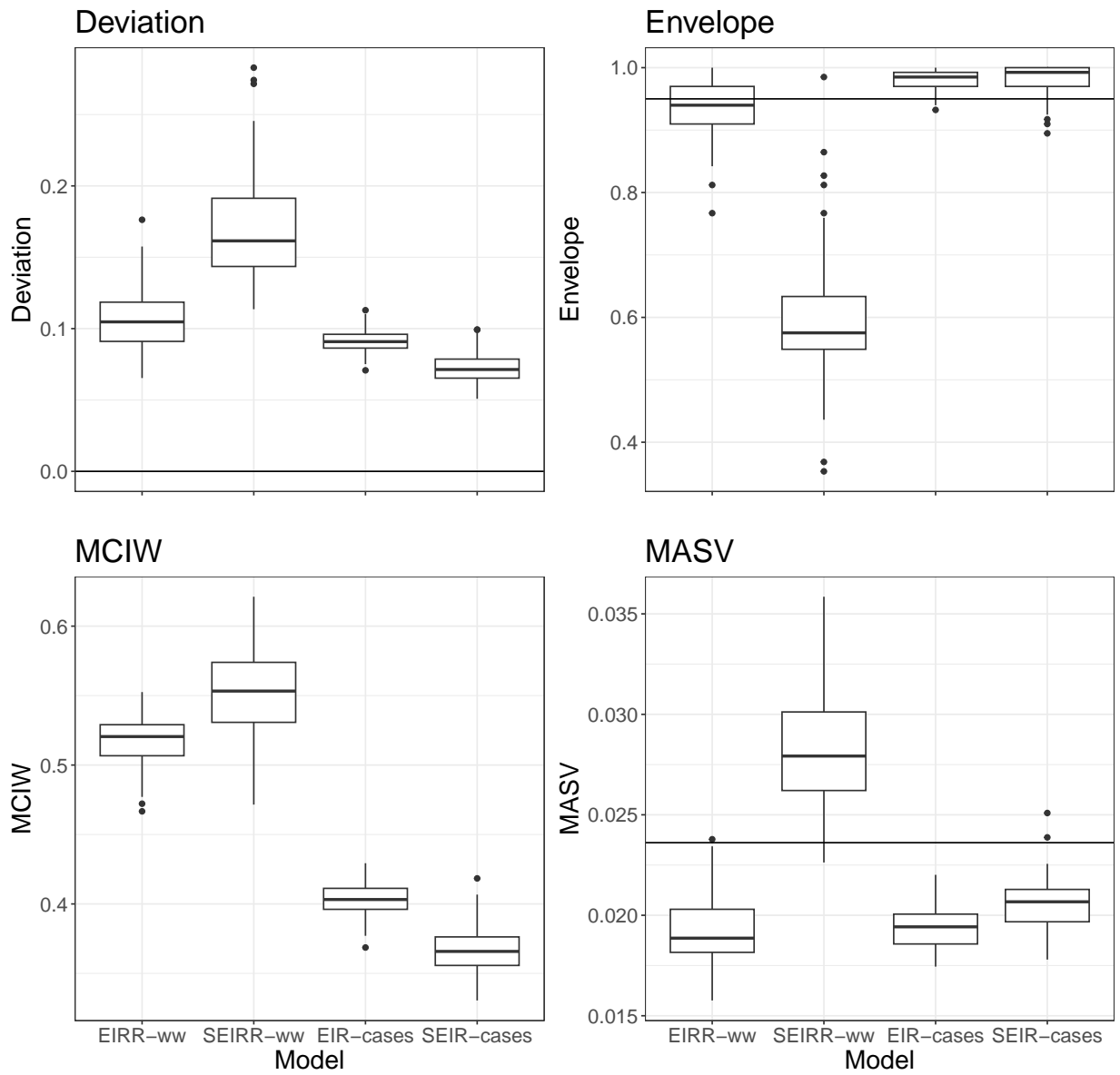


Figure A10: Frequentist metrics for all models using 95% CI as opposed to 80% CI as in the main text. The ideal Envelope is now 0.95. See Figure 3 in the main text for descriptions of the metrics.

Frequentist Metrics (Sensitivity Analysis)

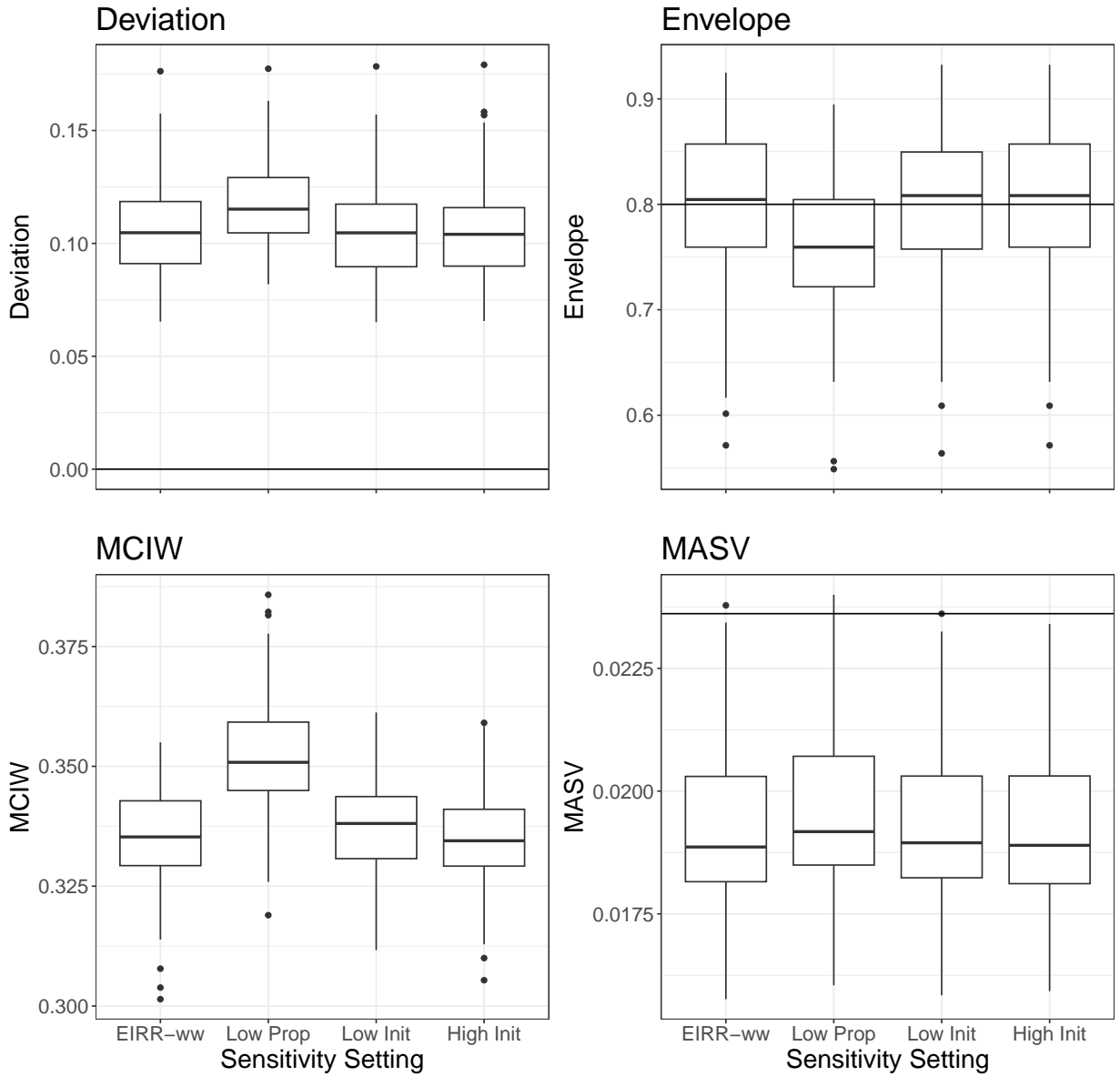


Figure A11: Frequentist metrics for performance of the EIRR-ww model using mis-specified priors. See Figure 3 in the main text for descriptions of the metrics.

Frequentist Metrics (State of the Art)

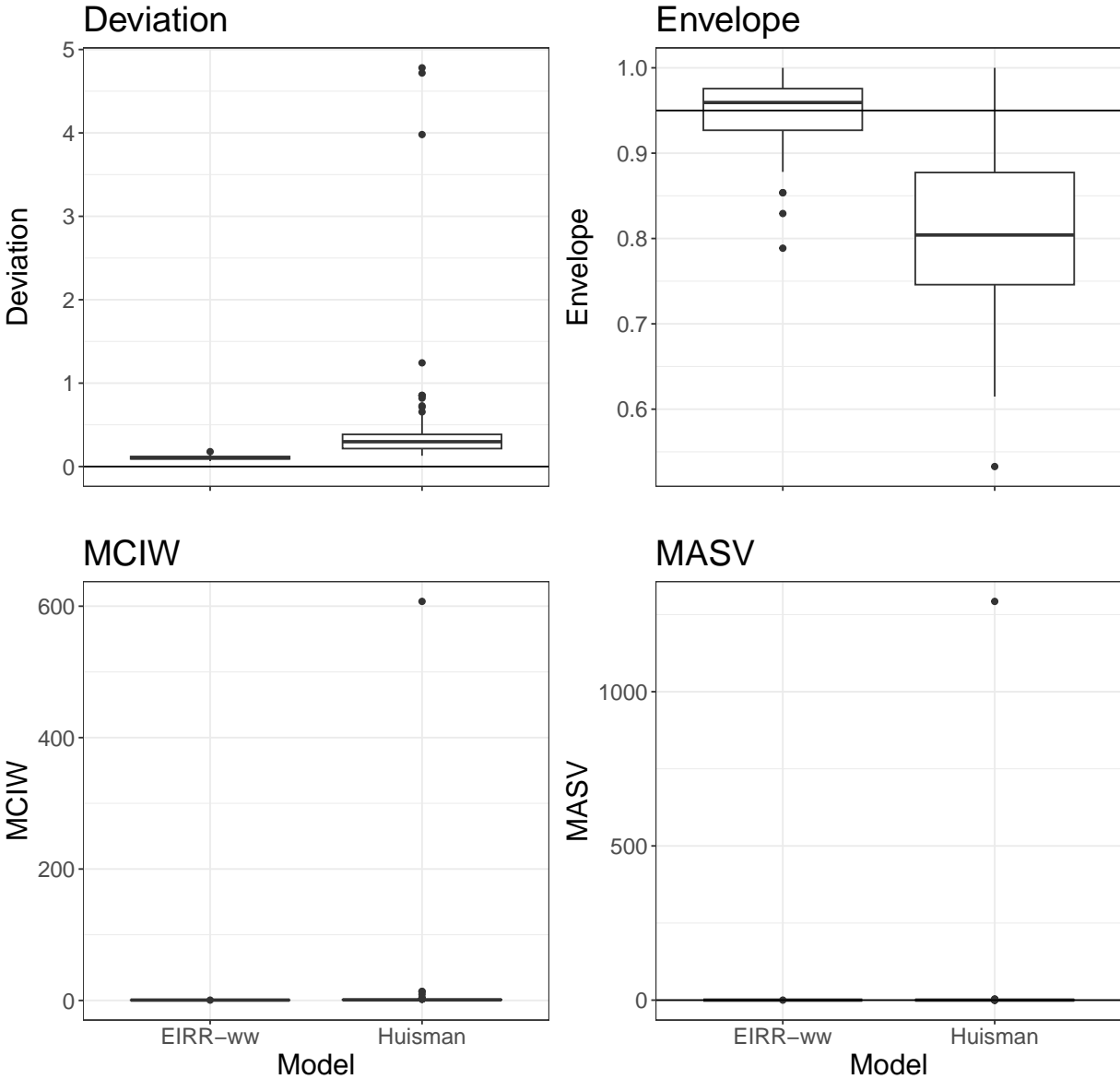


Figure A12: Frequentist metrics for performance of the EIRR-ww model compared to the Huisman et al. (2022) method. See Figure 3 in the main text for descriptions of the metrics. For one simulation, the deviation of the Huisman model was 600, this was removed from the graph to facilitate visualization.

A.2.6 Computational performance of closed solution versus ODE solver

Setting	Closed Form Time	Numerical Solver Time
Fitting to day data	855 seconds	872 seconds
Fitting to half-day data	3567 seconds	4260 seconds

Table A3: Comparing performance of closed form solution to ODE system versus an ODE solver.

A.2.7 Calculating Initial Conditions for Los Angeles, CA

We used the case data to create a rough guess for the initial conditions for our EIRR-ww and EIR-cases models. We assumed the total number of individuals in Los Angeles County in the E and I compartments was equal to the last 11 days before the start of the observation period (the sum of the average latent period and average infectious period) of reported cases multiplied by 5 (i.e. an under-reporting rate of 0.2). We then split this total so that two thirds went to the I compartment and one third went to the E compartment. We then took the 18 days (the average duration in the $R1$ compartment) before the last 11 days, multiplied the total cases by 5 and assumed that this was the number of individuals in the $R1$ compartment. Los Angeles County has about 10 million people total, so we multiplied these counts by 0.48 for the final compartment counts, as the JWPCP plant serves 4.8 million people. For the initial effective reproduction number, we chose a prior centered around 2, this was based on previous estimates of the effective reproduction number during this time using case data [13]. The final priors are displayed in the table below.

Table A4: EIRR-ww/EIR-cases Priors for Los Angeles, CA.

Parameter	Prior	Prior Median (95% Interval)
$E(0)$	Normal(2995, 0.05)	2995.00 (2994.90, 2995.10)
$I(0)$	Normal(5990, 0.05)	5990.00 (5998.90, 5990.10)
$R1(0)$	Normal(11055, 0.05)	11055.00 (11054.90, 11055.10)
R_0	Log-Normal(log(2), 0.1)	2 (1.64, 2.43)

A.2.8 Additional estimates of R_t for SARS-CoV-2 in Los Angeles, CA

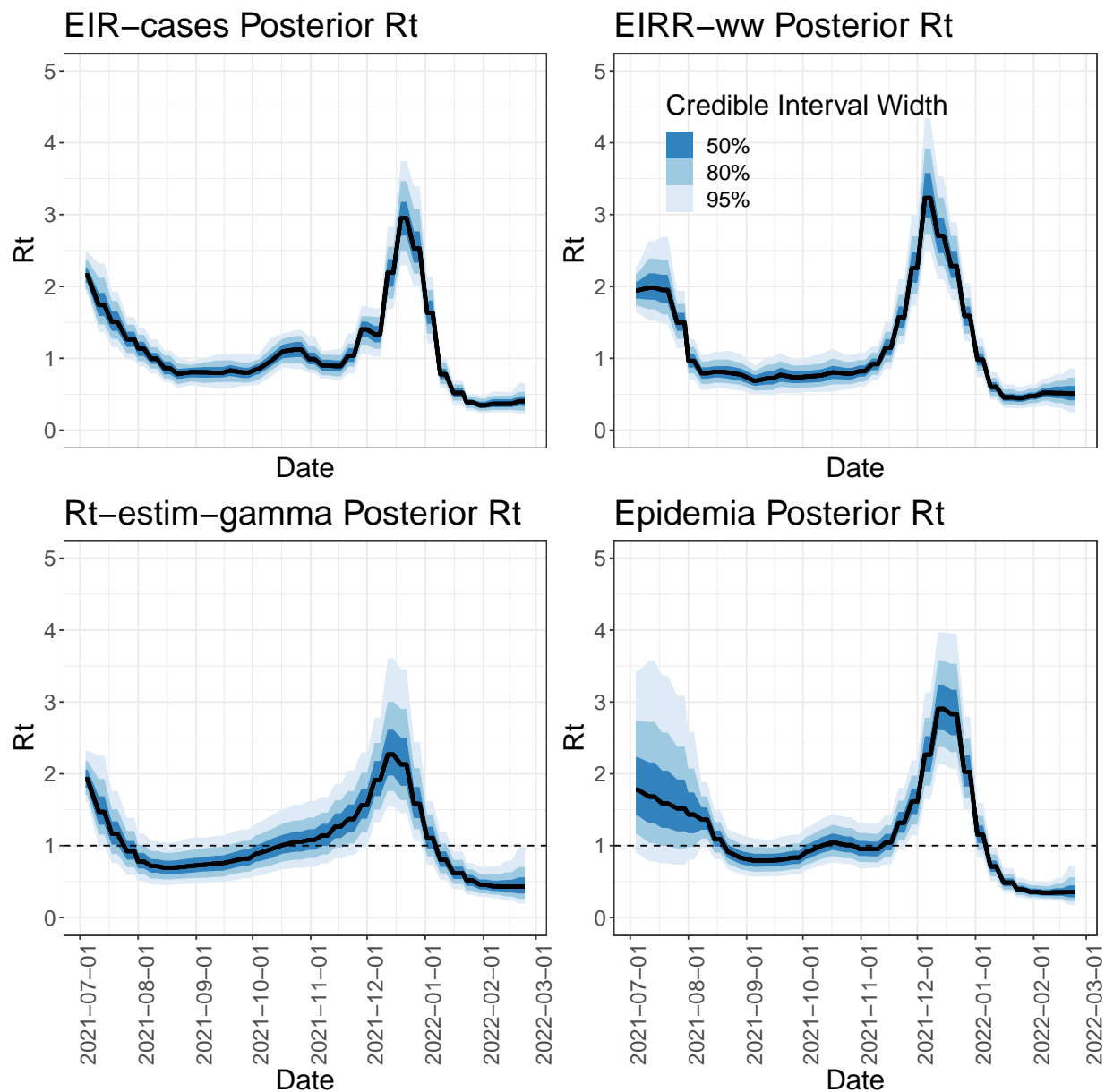


Figure A13: Posterior estimates of the effective reproduction number for the SARS-CoV-2 epidemic in Los Angeles, CA. Blue bars from dark to light represent 50, 80, and 95% credible intervals. Black lines represent posterior medians. EIRR-ww model is fit to wastewater data. EIR-cases and epidemia are fit to cases alone. R_t -estim-gamma is fit to cases and uses total diagnostic tests as a covariate.

A.2.9 Estimates of the case detection rate for SARS-CoV-2 in Los Angeles, CA

We can use the the posterior samples of $C(t_u)$ (the cumulative incidence at time t_u) produced by the EIRR-ww model to estimate the case detection rate, i.e., the proportion of new infections which are observed as reported cases. For each posterior sample, we calculate a

sample of the case detection rate as

$$\kappa_u = O_u / (C(t_u) - C(t_{u-1})),$$

where O_u is the number of new cases observed in the time period $(t_{u-1}, t_u]$. Note that κ_u is a function of the total diagnostic tests administered during the time period, thus, it is also interesting to look at the case detection rate normalized by the number of diagnostic tests. We call this normalized case detection rate *rho*, defined as

$$\epsilon_u = \kappa_u / D_u,$$

where D_u is the total number of diagnostic tests (both positive and negative) administered in the time period $(t_{u-1}, t_u]$. Posterior estimates of the case detection rate and normalized case detection rate of SARS-CoV-2 from Los Angeles, CA are shown in the figure below.

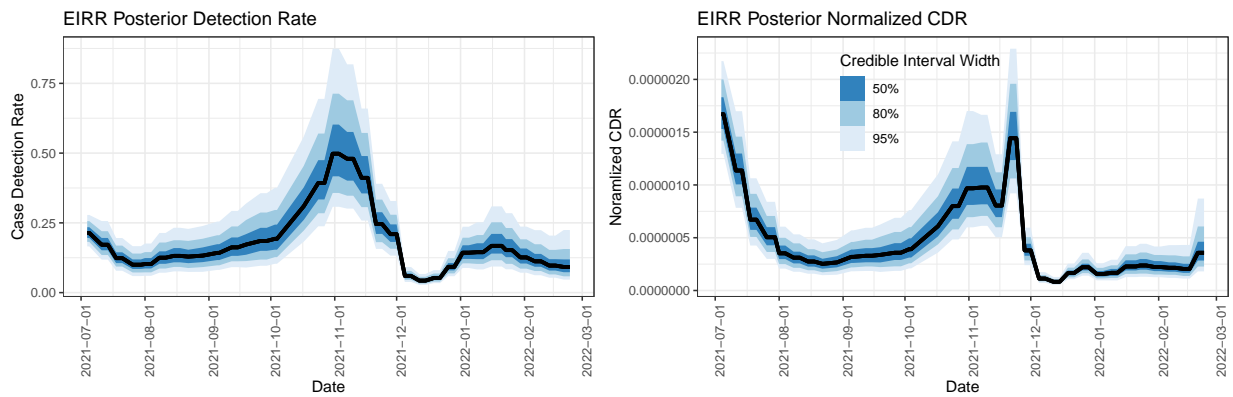


Figure A14: Posterior summaries of the case detection rate and case detection rate normalized by total diagnostic tests for SARS-CoV-2 in Los Angeles, CA. Posterior summaries of the number of new infections taken from wastewater, and the observed weekly case counts, are used to create posterior summaries of the case detection rate.

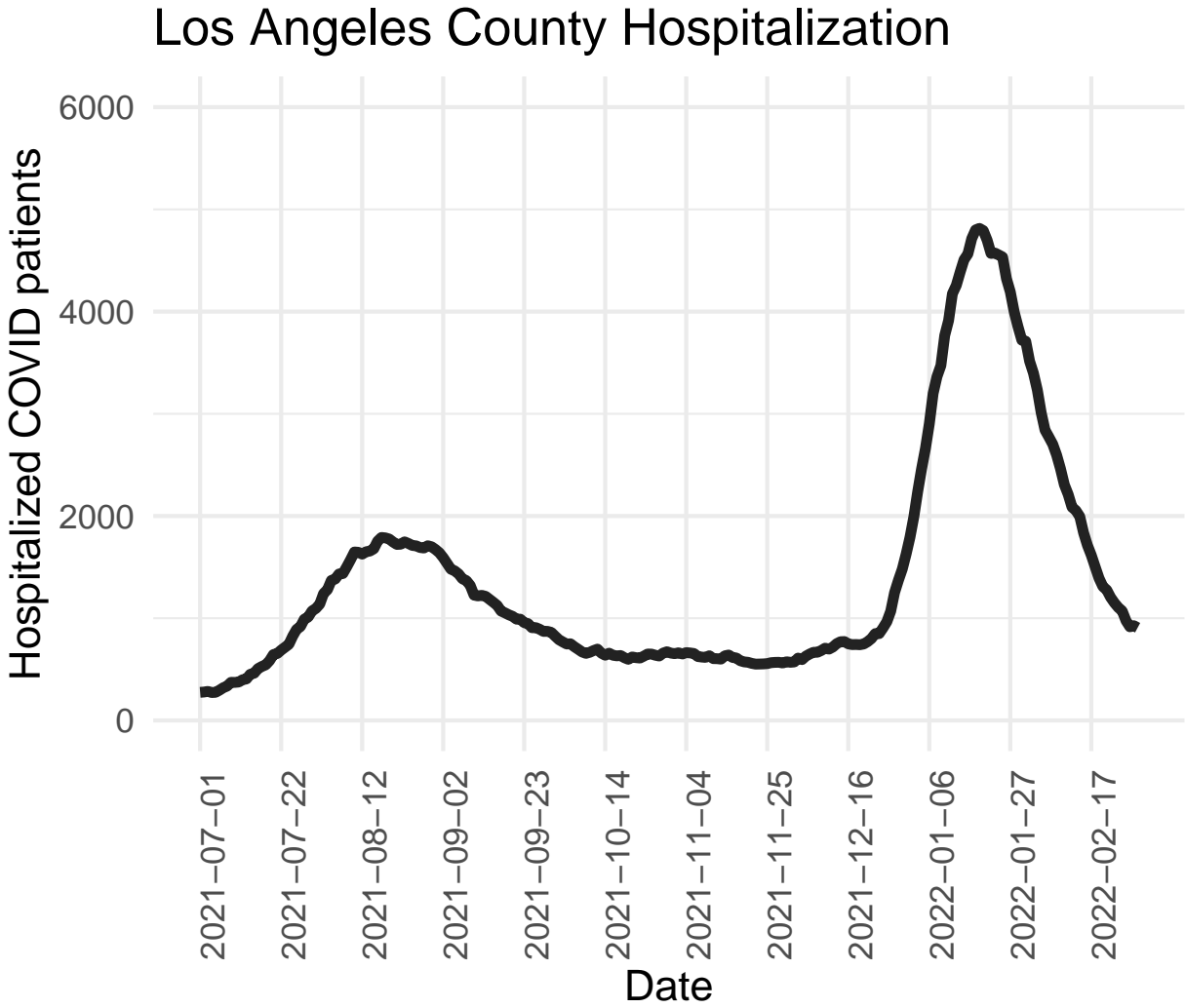


Figure A15: Time series of patients hospitalized with SARS-CoV-2 for Los Angeles County, CA.